

---

# PRECONDITIONING NATURAL AND SECOND ORDER GRADIENT DESCENT IN QUANTUM OPTIMIZATION: A PERFORMANCE BENCHMARK

---

**Théo Lisart-Liebermann**

theo.lisart@itwm.fraunhofer.de

Arcesio Castañeda Medina

arcesio.castaneda.medina@itwm.fraunhofer.de

Fraunhofer ITWM, 67655 Kaiserslautern, Germany

April 24, 2025

## ABSTRACT

The optimization of parametric quantum circuits is technically hindered by three major obstacles: the non-convex nature of the objective function, noisy gradient evaluations, and the presence of barren plateaus. As a result, the selection of classical optimizer becomes a critical factor in assessing and exploiting quantum-classical applications. One promising approach to tackle these challenges involves incorporating curvature information into the parameter update. The most prominent methods in this field are quasi-Newton and quantum natural gradient methods, which can facilitate faster convergence compared to first-order approaches. Second order methods however exhibit a significant trade-off between computational cost and accuracy, as well as heightened sensitivity to noise. This study evaluates the performance of three families of optimizers on synthetically generated MaxCut problems on a shallow QAOA algorithm. To address noise sensitivity and iteration cost, we demonstrate that incorporating secant-penalization in the BFGS update rule (SP-BFGS) yields improved outcomes for QAOA optimization problems, introducing a novel approach to stabilizing BFGS updates against gradient noise.

# 1 Introduction

Variational Quantum Algorithms (VQAs) are considered the main candidate for near-term quantum advantage [1–5]. These algorithms employ an iterative process that leverages the strengths of both quantum and classical computing. The approach involves evaluating an objective function using a parameterized quantum circuit on quantum hardware, and then utilizing a classical optimization routine to refine the results. This hybrid strategy is particularly valuable when the objective function can be efficiently computed on quantum hardware, potentially offering significant performance advantages across various applications: quantum chemistry [6–9], combinatorial problems [10–13], simulation [14–16], control [17–19], quantum machine learning (QML) [20, 21], numerical methods subroutines [22].

The performance of these applications is heavily influenced by the classical routine’s ability to identify a satisfactory approximation of the global optimum. This capability depends on the selection of an optimal optimization algorithm and the underlying optimization landscape associated with the objective function, which can be compromised by various factors. In particular, the so-called barren plateaus (BP) lead to entire regions of vanishing gradients as the result of sources such as noise [23], type of cost-function [24], and ansatz design and presence of entanglement [25, 26]. Although recent research has shown that the origin of BP from the ansatz structure can be avoided for a large class of problems [27–30], poor gradient quality remains a practical concern in many cases [31].

Optimization of VQA models in realistic settings is hampered by the inherent non-convexity of their objective functions [5, 32, 33] and noisy gradient estimates [34]. This dual challenge undermines theoretical guarantees of convergence for traditional optimization methods [35–37], and the classical optimizer must be tailored to the specific problem.

Success in optimizing parametric quantum circuits relies on tradeoffs between minimizing quantum hardware calls, number of iterations and performance in noisy function calls. Previous efforts focused on benchmarking gradientless (zero-order order) and first order methods. Thus, for example, authors in [38] approach noisy objective function evaluation using stochastic methods, in particular the Simultaneous Perturbation Stochastic Approximation (SPSA) [39] and second order extension [40]. On the other hand, in [41] an extensive study of *SciPy* [42] implementations of popular optimizers is provided, covering stochastic gradient methods, zero-order and first order methods. This last work extends on [43], which focused on establishing best practice for gradient-free methods in controlled noisy emulators. The latter argues that specifically tuned optimizers are crucial and will be needed even in the presence of usable error correction schemes, justifying the need for improvements using hyper-parameter fine

tuning using more advanced surrogate models [44, 45]. Within those studies, particular attention was brought to the definition of relevant cost models designed to balance empirical efficiency (or direct runtime cost) and solution accuracies relevant for the specific needs of quantum computing.

A rich literature of methods from classical optimization has emerged in the context of VQA-based quantum optimization [46–49]. For reference, we can list the Nelder-Mead simplex algorithm [50], SPSA [51], collective and swarm optimization (ant-based, particle-swarm), Bayesian optimization, gradient-based reinforcement learning, Powell’s method, Conjugate Gradient, Constrained Optimization by Linear Approximation (COPYLA), Sequential Least Squares Programming (SLSQP), Broyden–Fletcher–Goldfarb–Shanno (BFGS), and Byrd-Omojokun Trust Region Sequential Quadratic Programming (trust-constr) [52]. Another family of promising methods comes from the field of machine learning, which has seen significant success over the last two decades. Namely gradient-based methods such as Stochastic Gradient Descent (SGD), Adaptive Gradient Algorithm (AdaGrad) [53], Root Mean Square Propagation (RMSProp) [54], Follow the Regularized Leader (FTRL) [55], Adam, Adamax, Nadam, and AMS-Grad [56–58]. Machine-learning centric methods have been ranked for quantum optimization problems in [41].

Systematic testing of cutting-edge quasi-Newton methods has not been as thoroughly examined as zero-order and first-order methods. Benchmarking different variants of these methods, using distinct Hessian matrix approximations and alternative shot noise mitigation strategies, can provide better alternatives for VQAs. Thus, for example, although the Davidon-Fletcher-Powell (DFP) method [59], which predates BFGS and its limited memory variant [60], has been shown to be less accurate and stable than its successor, fine-tuned DFP could potentially lead to faster convergence due to its more aggressive Hessian approximation. Other methods, like the The Symmetric Rank One (SR1) method [61], offer a flexible Hessian matrix approximation, particularly in situations where well-posedness cannot be guaranteed. Another overlooked approach is the quasi-Newton update based on the Conjugate Gradient (NCG) Hessian approximation [62], which inherits the advantages of CG for quasi-Newton updates while offering improved scaling and memory usage, although tends to perform poorly in non-convex geometries. An alternative strategy for leveraging second-order information at key points in parameter space involves applying a contemporary approach that incorporates a gradient quality metric when updating the BFGS algorithm (SP-BFGS) [63]. By penalizing the update, this method has a stabilizing effect on the Hessian approximation, enhancing overall robustness and dynamical properties. The technique seamlessly interpolates between first- and second-order methods, thereby preventing accumulation of errors in the Hessian approximation, and generalizes BFGS updates to noisy function evaluations.

Second order methods scales the step size of the Newton update according to the Hessian matrix information. It is known however that local gradients evaluations are not the best possible update direction [64, 65]. Natural Gradient Descent (NGD) use the Fisher information matrix (FIM) to precondition the update step, as the natural direction of greatest change. Under this conceptual framework, the Quantum Natural Gradient (QNG) updates the parameters in the direction of biggest change according to Quantum Information Geometry [66] through a block approximation of the Fubini-Study metric tensor, also known as the Quantum Fisher Information Matrix (QFIM). Contrary to the classical natural gradient method, the QFIM is not explicitly linked to the Hessian of the objective function, exploring the geometry of the parameter space in probability space. This approach can be considered as a preconditioned gradient update.

Building on the principles of Quantum Natural Gradient (QNG), various methods have been proposed to enhance the efficiency of Quantum Fisher Information Matrix (QFIM) evaluations. Notably, the introduction of Quantum-Natural Stochastic Perturbation Synthesis Algorithm (QNPSA) in [67] represents an initial step in this direction. More recently, momentum-based and Broyden-type methods have been developed to offer gradient-based QFIM approximations, exemplified by the qBroyden and qBang algorithms [68]. The inclusion of stochastic methods such as SPSA, 2SPSA, and QNPSA provides valuable insight into the impact of Hessian and QFIM approximations on optimizing quantum circuits, with experimental relevance established [69–71]. Furthermore, other the Random Coordinate Descent (RCD) algorithm [72, 73], have demonstrated improved performance for PQC’s optimization, which we verify. We use the stochastic methods as a reference point for comparing methods.

The three main categories of methods - quasi-Newton, natural gradient, and stochastic techniques - serve as the foundation for our examination of second-order methods in quantum optimization, which are summarized in Tab. 1.

| Family                    | Method           |
|---------------------------|------------------|
| Second order quasi-Newton | NCG              |
|                           | BFGS             |
|                           | DFP              |
|                           | SR1              |
| Quantum Natural Gradient  | SP-BFGS          |
|                           | QNG (block-diag) |
|                           | qBroyden         |
|                           | qBang            |
| Stochastic                | m-QNG            |
|                           | SPSA             |
|                           | 2SPSA            |
|                           | QNPSA            |
|                           | RCD              |

Table 1: Scope of studied methods within this work

Most of these methods, excluding pure QNG, demand meticulous tuning of hyperparameters to achieve optimal results. The literature on hyper-parameter optimization is extensive, with numerous techniques available, including genetic algorithms [74], bandit-based approaches [75], random search [76], and autoML [77]. One method that stands out for its ability to handle low-dimensional spaces is Bayesian optimization [78, 79], which proves particularly effective when each model evaluation is computationally intensive. In this study, the hyper-parameter space is explored through successive iterations of Bayesian optimization, resulting in a comprehensive coverage of both randomly sampled and optimal scenarios for each hyperparameters optimization run.

The primary concern for evaluating combinatorial solvers is not their inherent ability to find optimal solutions, but rather their capacity to identify solutions that are satisfactory for specific applications or domains. The ultimate goal is to determine how efficiently and reliably a solver can locate an acceptable solution. Consequently, the performance of these optimizers is typically measured against quality-to-cost metrics. Within this study, our focus lies on understanding solver dynamics and solution quality, which can be quantified through various indicators. Specifically, we consider the pairwise Hamming distance associated with bitstring solutions [80], as well as overall convergence ratios that estimate the success probability of the methods employed. Additionally, standard metrics such as objective function values, quantum calls, overall walltime, and average iteration to convergence are also taken into account.

For the second-order quasi-Newton family, our results suggest that the choice of Hessian approximation is crucial for quasi-Newton methods’ ability to achieve acceptable solutions. Specifically, DFP methods offer higher convergence probabilities and solution quality at the cost of numerical instability. In contrast, more dynamic rank-1 methods like SR1 do not provide significant improvements. However, SP-BFGS offers reasonable convergence ratios while also stabilizing BFGS and DFP Broyden updates, although this comes with the added complexity of two additional hyperparameters to fine-tune.

For quantum natural gradient (QNG) methods, in general, principal appeal is the absence of hyper-parameter tuning in general, this is however not the case for its approximate variants, which often require challenging hyper-parameter tuning. However, the addition of momentum in QNG does improve convergence speed drastically, but reduces significantly convergence rates particularly at higher problem sizes. Notably, QNG-type methods exhibit better overall convergence consistency compared to quasi-Newton methods, suggesting that cheaper QFIM estimation remains a worthwhile area of investigation.

Stochastic methods overall require parameter tuning for an appreciable performance, overall we find that QN-SPSA helps at low dimensions convergence rates. 2SPSA however requires intensive tuning to scale, which is not

necessarily possible. At convergence, the introduction of second order estimators do drastically increases convergence speed, but at the cost of drastic increase in variability in performances.

This paper is organized as follows: In Sec. 2, we provide a detailed introduction to the theoretical framework underlying the studied methods, including an overview of the standard MaxCut problem and its Quantum Approximate Optimization Algorithm (QAOA) implementation. We then devote Sec. 2.2 to an in-depth examination of the methods listed in Tab 1, followed by a presentation of Bayesian hyper-parameter fine tuning techniques in Sec. 2.5. The performance metrics and context for hyperparameters fine tuning are specified in Sec. 2.6. Finally, the obtained results are discussed in full detail in Sec. 3, while our key observations and suggestions for future work on applying second-order methods for quantum circuit optimization are presented in Sec. 4.

## 2 Theoretical framework

The quantum-classical optimization loop, appearing in quantum algorithms such as QAOA, Variational Quantum Eigensolvers (VQE) [9], Harrow–Hassidim–Lloyd (HHL) [81], sensing [82, 83], and quantum machine learning (QML) [84], rely on the definition of quantum ansatzs, whose tunable parameters are defined on a parameterized quantum circuit [3, 9, 85]. In this section, we introduce the MaxCut problem and the associated QAOA circuit forming the basis of the numerical investigation, we then go into details of the second order quasi-Newton methods and quantum natural gradient methods.

### 2.1 MaxCut and the QAOA algorithm

Given a weighted graph  $G = (V, E, w)$ , where  $V$  represents the set of vertices,  $E$  denotes the set of edges, and  $w$  is a weight function mapping each edge to a positive real number, the MaxCut problem seeks to partition the vertex set  $V$  into two non-overlapping subsets  $S$  and its complement  $\bar{S} = V \setminus S$ , with the goal of maximizing the total weight of edges between these two subsets. By defining binary variables  $z_i \in \{0, 1\}$  for each vertex  $i \in V$ , the problem’s objective function can be formally expressed as:

$$\text{MaxCut}(G) = \max_{\mathbf{z} \in \{0,1\}^n} \sum_{(i,j) \in E} w_{ij} \cdot \frac{1}{2}(1 - z_i z_j), \quad (1)$$

where  $n = |V|$  is the number of vertices in the graph. To solve this problem using a quantum-classical approach, the cost function (1) is re-expressed as a minimization problem and the Quantum Approximate Optimization Algorithm (QAOA) method is employed as the solver. QAOA represents an  $n$ -qubit Ansatz Trotterization of the adiabatic evolution as described in [12], with its precision

controlled by a positive parameter  $p$ , which determines the number of mixer-problem unitary applications. To establish the problem’s unitary operator, we directly translate the cost function into Pauli-Z operators acting on each qubit:

$$\hat{P} = \sum_{(i,j) \in E} w_{ij} \cdot \frac{1}{2}(\hat{Z}_i \hat{Z}_j - I). \quad (2)$$

The Quantum Approximate Optimization Algorithm (QAOA) Ansatz is defined as:

$$|\gamma, \beta\rangle = U_B(\beta_p)U_P(\gamma_p)\dots U_B(\beta_1)U_P(\gamma_1)|+\rangle^{\otimes n}, \quad (3)$$

where the problem and mixer generators are given by  $U_P(\gamma) = e^{-i\gamma P}$  and  $U_B(\beta) = e^{-i\beta B}$ , with the mixer Hamiltonian and  $B = \sum_{i=1}^n X_i$ , respectively. This establishes a parameter space that spans  $2p$  real numbers,  $\gamma = (\gamma_1, \dots, \gamma_p)$  and  $\beta = (\beta_1, \dots, \beta_p)$ .

With  $p$  fixed, the QAOA algorithm estimates the solution by employing a classical optimizer to identify the optimal set of parameters  $\theta \equiv \{\gamma, \beta\}$  that minimizes:

$$f(\theta) = \min_{\theta} \langle \theta | P(z) | \theta \rangle, \quad (4)$$

utilizing the Pauli-strings expectation values computed on a quantum processor or emulator.

### 2.2 Methods

For functions with non-exponential decay or complex landscapes featuring multiple critical points, first-order methods often struggle to converge effectively. In contrast, second-order methods utilize the Hessian matrix to scale the step size according to the landscape’s geometric characteristics and adjust the direction of the gradient based on curvature information. This allows for improved convergence in flat areas or heavily bumpy surfaces with numerous critical points.

Starting from the Taylor expansion  $f(\theta_i) \approx f(\theta_i) + (\theta_{i+1} - \theta_i)^T \nabla_{\theta} f(\theta_i) + \frac{1}{2}(\theta_{i+1} - \theta_i)^T H(\theta_{i+1} - \theta_i)$ , the second-order Newton update rule with step size  $\alpha$  can be derived as follows:

$$\theta_{i+1} = \theta_i - \alpha H^{-1} \nabla_{\theta} f(\theta_i), \quad (5)$$

By solving for the critical point using the inverse Hessian  $H^{-1}$ , the optimization step can be performed through a standard line search along the search direction  $p_i = -H_i^{-1} \nabla_{\theta} f(\theta_i)$ . Further improvements can be achieved by incorporating problem-adapted linear updates or more efficient search methods, such as Trust Region techniques [86, 87]. However, if the function is not strongly convex, enforcing the Wolfe condition becomes essential

to ensure stability of the line search procedure. The sub-optimization fulfills this condition when the Amijo rule and the curvature condition are met:

$$f(\theta_i - \alpha_i p_i) \leq f(\theta_i) + c_1 \alpha_i p_i^T \nabla_\theta f(\nabla_i) \quad (6)$$

$$-p_i^T \nabla_\theta f(\theta_i + \alpha_i p_i) \leq -c_2 p_i^T \nabla_\theta f(\theta_i) \quad (7)$$

These conditions provide heuristical upper and lower bounds to the optimal choice of step size in the line search. Typical values for hyperparameters  $c_1$  and  $c_2$  are  $10^{-4}$  and  $0.9$ , respectively, although they should ideally be tuned empirically.

Moreover, the positiveness of the Hessian imposes additional constraints on the direction of search, such as the curvature condition  $p_i^T y_i > 0$ , where  $y_i = \nabla_\theta f(\theta_{i+1}) - \nabla_\theta f(\theta_i)$ . In this study, we employ a simple line search and backtracking with a maximum number of iterations. The conditions (6) and (7) are iteratively checked to reduce the step size  $\alpha$  by  $\beta$  for a given  $(c_1, c_2)$  pair until either the maximum backtracking iteration is reached or the conditions are satisfied.

In practice, direct use of Newton methods can be computationally expensive due to the need to compute the full Hessian at each iteration and handle instabilities with aggressive regularizations. For large matrices, explicit inversion of  $H$  can also be challenging if the matrix is dense [88]. In the context of VQAs, gradient and higher-order derivative estimations can be achieved using parameter-shift routines [89–91], introducing auto-differentiation approaches to gradient estimation in parametric quantum circuits.

### 2.3 Quasi-newton second order methods

Quasi-Newton methods address the limitations of Newton’s method by introducing inverse Hessian approximations,  $B_i = \tilde{H}_i^{-1}$ , that are based on the history of gradient evaluations. This results in more stable and efficient algorithms, with reduced computational costs from  $\mathcal{O}(n^3)$  to  $\mathcal{O}(n^2)$  for an  $n \times n$  Hessian matrix, irrespective of the specific Hessian approximation employed [87, 92].

These methods have been extensively studied in various fields and are represented by the well-known (L-)BFGS method [93], which has been applied to diverse quantum optimization problems [41, 43, 52, 94]. Other quasi-Newton methods include the Davidon-Fletcher-Powell (DFP) method, which is less robust but more efficient per iteration; the Symmetric Rank One (SR1) method [61], which improves upon the dynamical scaling of Hessian approximations; and the Quasi-Newton Conjugate Gradient (NCG) [95], which employs the conjugate gradient method for the Hessian approximation. Broyden’s method families [96] are a generalization of these methods and will be discussed in Sec. 2.4 in the context of quantum natural gradient methods.

Quasi-Newton methods typically begin with an initial guess, often the identity matrix, and iteratively build upon it to develop a Hessian approximation. The accuracy of these approximations relies heavily on the quality of the Hessian update rule. Below, we provide a brief overview of some standard quasi-Newton approximations. For more detailed descriptions, please refer to the references [52, 60, 93].

#### 2.3.1 Davidon-Fletcher-Powell (DFP)

Introduced by Davidon in 1959, the DFP update rule is a seminal contribution to quasi-Newton methods. The inverse Hessian approximation, where the update direction is given as  $s_i = \alpha p_i$ , is derived from the Sherman–Morrison–Woodbury formula [52]:

$$B_{i+1} = B_i + \frac{s_i s_i^T}{s_i^T y_i} - \frac{B_i y_i y_i^T B_i}{y_i^T B_i y_i}, \quad (8)$$

Although the DFP method was largely superseded by subsequent methods, it can outperform the BFGS method in specific cases of objective function non-linearities. This is particularly evident in situations involving noisy gradient evaluations, as the DFP method exhibits reduced sensitivity to initial conditions and improved recovery from poor Hessian estimation [52].

#### 2.3.2 Broyden-Fletcher-Goldfarb-Shanno (BFGS)

Developed in an effort to find a better inverse Hessian approximation from the DFP method, the BFGS method has been empirically shown to be the best known quasi-Newton update formula [52]. The rank-2 update method takes the form:

$$B_{i+1} = B_i + \left(1 + \frac{y_i^T B_i y_i}{s_i^T y_i}\right) \frac{s_i s_i^T}{s_i^T y_i} - \frac{s_i y_i^T B_i + B_i y_i s_i^T}{s_i^T y_i}. \quad (9)$$

The BFGS update is derived similarly to the DFP method, introducing a quadratic model of the Hessian. For a displacement  $s_i$  and variation in gradients  $y_i$ , the secant condition requires that the new approximation maps  $s_i$  and  $y_i$  together:  $B_{i+1} s_i = y_i$ , which is known as the secant condition.

#### 2.3.3 Symmetric Rank One (SR1)

In SR1 method the inverse Hessian is given by the rank-1 symmetric update:

$$B_{i+1} = B_i + \frac{(s_i - B_i y_i)(s_i - B_i y_i)^T}{(s_i - B_i y_i)^T y_i}, \quad (10)$$

which maintains matrix symmetry and satisfies the secant condition. However, it does not guarantee positive definiteness, implying that a line-search or trust region

method should be employed in conjunction with this update to ensure stability [52].

### 2.3.4 Quasi-Newton Conjugate Gradient (NCG)

The Conjugate Gradient (CG) algorithm occupies a middle ground between steepest descent methods and quasi-Newton approaches [95]. A significant advantage of CG methods is their ability to operate without explicit storage of matrices, thus enhancing both memory efficiency and computational speed.

Mathematically, the update rules for conjugate gradient methods are defined by:

$$x_{i+1} = x_i + \alpha p_i, \quad (11)$$

where the direction of the line search is given by  $p_i = -\nabla_\theta f(\theta_i) + \beta_i p_{i-1}$ .

Variations among different CG methods arise from the selection of the multiplier  $\beta_i$  at each iteration, which forms the core of the line-search algorithm. The quasi-Newton Conjugate Gradient (NCG) method builds upon standard CG approaches by incorporating an inexact line search and leveraging the quasi-Newton condition instead of the conjugacy condition in the update rule. Furthermore, NCG methods utilize second-order approximations to derive both step sizes and search directions. In the context of quantum optimization, NCG approaches permit the relaxation of the quadratic condition through the use of reset rules.

In an inexact line-search scenario, the Quasi-Newton condition can be leveraged to derive a  $\beta_i$  with  $\mathbf{p}_i = -\tilde{H}_i^{-1} g_i$ , where  $g_i = \nabla_\theta f(\theta_i)$ .

Scaled quasi-Newton update with inexact line search [62]:

$$\beta_i = \frac{y_i^T g_i - (1/s_i) p_i^T g_i}{y_i^T d_{k-1}}, \quad (12)$$

Similarly to SP-BFGS method, local evaluation of gradient quality interpolates continuously between the most relevant method depending on second order metrics, in the case of CG updates, Perry's strategy as the factor ( $s_i \rightarrow 1$ ) and coincides with the Hestenes and Stiefel's strategy when ( $s_i \rightarrow \infty$ ). Various quasi-Newton approximations can be used in evaluating  $\beta_i$ , standards ones can be found in the original paper [95]

### 2.3.5 The Secant-Penalized BFGS (SP-BFGS)

This approach endeavors to mitigate the influence of local dependence on the accuracy of gradient estimation by introducing an adaptive parameter  $\beta_i$ , derived from the curvature condition ( $-\beta_i^{-1} < s_i^T y_i$ ), which smoothly transitions between a full BFGS step (as  $\beta_i \rightarrow \infty$ ) and a standard gradient descent update (as  $\beta_i \rightarrow 0$ ) [63, 97].

The update rule for the SP-BFSG method is derived from the integration of penalty terms into the BFGS update rule [63] and can be expressed as follows:

**Algorithm 1** SP-BFGS implementation, with the Amijo-Wolf backtracking. *compute\_linear* function is the expression in adapting  $\beta_i$  with interception or noise model in Eq. 16

---

```

1: Input:  $f, \beta\_compute\_linear, x_{init}, \alpha, \beta_{reduce}, c_0, c_1, N_0, N_s, MAXIT$ 
2: Output:  $x, best\_value$ 
3:  $x \leftarrow x_{init}$ 
4:  $i \leftarrow 0$ 
5:  $H_i \leftarrow$  Identity Matrix
6: while  $i < MAXIT$  do
7:    $\nabla_i \leftarrow \nabla_\theta f(x)$ 
8:   if  $\|\nabla_i\| < tol$  then
9:     break
10:  end if
11:   $p_i \leftarrow -H_i \cdot \nabla_i$ 
12:  while not satisfying Armijo-Wolfe condition do
13:    if  $f(x + \alpha p_i) \leq f(x) + c_0 \alpha \cdot \nabla_i^T p_i$  then
14:      break
15:    end if
16:    if  $-p_i^T \nabla_\theta f(x + \alpha p_i) \leq -c_1 p_i^T \nabla_i$  then
17:      break
18:    end if
19:     $\alpha \leftarrow \beta_{reduce} \cdot \alpha$ 
20:  end while
21:   $x_i \leftarrow x + \alpha p_i$ 
22:   $s_i \leftarrow x_i - x$ 
23:   $\nabla_{i+} \leftarrow \nabla f(x_i)$ 
24:   $y_i \leftarrow \nabla_{i+} - \nabla_i$ 
25:   $\beta_i \leftarrow \beta\_compute\_linear(N_0, N_s, s_i)$ 
26:   $proj \leftarrow s_i^T \cdot y_i$ 
27:   $\gamma_i \leftarrow \frac{1}{proj + \frac{1}{\beta_i}}, \quad \omega_i \leftarrow \frac{1}{proj + \frac{2}{\beta_i}}$ 
28:   $H_{ns} \leftarrow (I - \omega_i (s_i \odot y_i)) \cdot H_i (I - \omega_i (y_i \odot s_i))$ 
29:   $H_{nc} \leftarrow \omega_i \cdot \left( \frac{\gamma_i}{\omega_i} + (\gamma_i - \omega_i) \cdot y_i^T \cdot H_i y_i \right) \cdot s_i s_i^T$ 
30:   $H_n \leftarrow H_{ns} + H_{nc}$ 
31:   $x \leftarrow x_i$ 
32:   $H_i \leftarrow H_n$ 
33:   $i \leftarrow i + 1$ 
34: end while
35: return  $x$ 

```

---

$$B_{i+1} = \left( I - \omega_i s_i y_i^T \right) B_i \left( I - \omega_i y_i s_i^T \right) + \quad (13)$$

$$\omega_i \left[ \frac{\gamma_i}{\omega_i} + (\gamma_i - \omega_i) y_i^T B_i y_i \right] s_i s_i^T, \quad (14)$$

where the parameters  $\gamma_i$  and  $\omega_i$  are defined by:

$$\gamma_i = \frac{1}{s_i^T y_i + \frac{1}{\beta_i}}, \quad \omega_i = \frac{1}{(s_i^T y_i + \frac{2}{\beta_i})}. \quad (15)$$

Adaptation of the parameter  $\beta_i$  relies on assumptions regarding the noise distribution that influences the gradient measurements. The original work proposed a rectified version of the Uniform Gradient Noise Bound, which

schedules the gradient measure linearly with respect to the continuous update parameter: ( $\beta_i \propto \|s_i\|_2$ ) [63]. To enhance update stability, an interception rule can be implemented when gradient information is insufficient for a proper update.

$$\beta_i = \max \left\{ N_s \|s_i\|_2 - N_0, 0 \right\} \quad (16)$$

We implement in Alg.1 the SP-BFGS procedure.

The phenomenological parameters  $N_0$  and  $N_s$  improve the stationary point dynamics by introducing a minimum gradient value beyond which noise dominates and second-order information is destroyed. They also scale the effects of noise. In this work, both hyperparameters are learned using Bayesian optimization.

## 2.4 Quantum natural gradient methods

Natural Gradient (NG) methods have been developed from the observation that the Euclidean metric is not always the most optimal description for a large class of objective functions. The exact form of the Newton update rule, as given in Eq. (17), implies an arbitrary choice of the  $l_2$  norm:

$$\theta_{i+1} = \underset{\theta \in \mathbb{R}^n}{\operatorname{argmin}} \left[ \langle \theta - \theta_i, \nabla_{\theta} f(\theta_i) \rangle + \frac{1}{2\alpha_i} \|\theta - \theta_i\|_2^2 \right]. \quad (17)$$

Then, by introducing a metric change,  $\|\cdot\|_2 \rightarrow \|\cdot\|_{g_{\theta}}$ , convergence can be improved by exploring changes in the model space instead of changes in the parameter space. The NG update rule, adapted from Eq. (5), is given by:

$$\theta_{i+1} = \theta_i - \alpha_i g^{-1}(\theta_i) \nabla_{\theta} f(\theta_i). \quad (18)$$

This natural preconditioning is invariant under parameter re-scaling and allows the gradient to always point towards the direction of greatest descent relative to the information geometry [64, 66, 67].

Within the quantum computing context, the Fubini-Study metric tensor,  $g^F$ , offers a natural metric corresponding to the variation of the model in probability space [98]. Inspired by Amari's NG descent [64] and the Berry connection between  $g^F$  and the Quantum Fisher Information Matrix (QFIM), namely  $F(=4g^F)$  [98, 99], the Quantum Natural Gradient (QNG) utilizes quantum information geometry to improve VQA optimization [66].

The QFIM Riemannian tensor, measuring the sensitivity of the model from the parametric space to the probability space  $p_{\theta}(x)$ , is given by:

$$F_{ij} = \sum_{x \in [N]} p_{\theta} \frac{\partial \log p_{\theta}(x)}{\partial \theta_i} \frac{\partial \log p_{\theta}(x)}{\partial \theta_j}, \quad (19)$$

where the sum extends over all possible  $x$  outputs. The corresponding The Fubini-Study metric is then given by:

$$g_{ij}^F(\theta) = \Re \left\{ \left\langle \frac{\partial \psi}{\partial \theta_i} \middle| \frac{\partial \psi}{\partial \theta_j} \right\rangle - \left\langle \frac{\partial \psi}{\partial \theta_i} \middle| \psi \right\rangle \left\langle \psi \middle| \frac{\partial \psi}{\partial \theta_j} \right\rangle \right\}. \quad (20)$$

Full estimation of the QFIM at every optimizer iteration is prohibitively expensive in quantum resources ( $\mathcal{O}(n_{\theta}^2)$  for  $n_{\theta}$  parameters), but through QNG's quantum circuit representation of the QFIM,  $g^F$  can be efficiently evaluated ( $\mathcal{O}(n_{\theta})$ ) by sub-circuit sampling, particularly within block-matrix and diagonal matrix approximations. These improvements can be, however, hindered by discarded inter-system correlations [100]. On the other hand, alternative methods and further approximations can also be introduced for avoiding QFIM explicit calculation altogether [101, 102]. In the following sections, we expose cheaper alternatives aiming at exploiting the QFIM by quasi-Newton inspired generalizations.

### 2.4.1 Momentum QNG methods

QNG improvements in convergence brought about by quantum information geometry are expected to be complementary to adaptive optimizers, such as Adam [66]. In moment-based techniques, preconditioning is evaluated based on a temporal average of the optimization function's behavior, rather than the local geometry of the quantum state space. A collection of QNG variants, including momentum averaging have been introduced recently [103]. We first revisit the conceptual framework underlying momentum optimization, before explaining some of these implementations.

The classic momentum update is a modern adaptation of Polyak's momentum method [104, 105], which modifies the Newton update rule as follows:

$$v_{i+1} = mv_i - \alpha H^{-1} \nabla_{\theta} f(\theta_i), \quad (21)$$

$$\theta_{i+1} = \theta_i + v_{i+1}. \quad (22)$$

Here,  $m \in [0, 1]$  is the momentum coefficient and  $v_i$  is the corrected update at iteration  $i$ , or velocity vector. Incorporating this physics-inspired momentum into parameter dynamics has a stabilizing effect in noisy and non-convex landscapes with large amounts of curvature, as it exponentially damps the oscillatory nature of gradient corrections. However, selecting an optimal momentum parameter, or introducing scheduling dynamics, is by itself another hyperparameter fine-tuning task [106, 107], which is computationally expensive and heavily problem-dependent.

Adaptive methods based on gradient history can approximate the Hessian and adapt multi-dimensional learning rates by naturally assigning higher rates to parameters with low-frequency geometrical features, while applying lower rates in directions with high curvature features.

Thus, for example, in ADAGRAD, the momentum update (21) follows the rule:

$$v_{i+1} = mv_i - \frac{\alpha}{\sqrt{\sum_{\tau=1}^i |\nabla_{\theta} f(\theta)|_{\tau}^2}} \nabla_{\theta} f(\theta), \quad (23)$$

where the denominator computes the  $l_2$  norm of all gradients at all previous iterations over a window of length  $\tau$ . This approach factors out gradient amplitudes into learning rates and exhibits an annealing effect. Additionally, it allows large magnitude variations in gradients while inheriting second-order update features as a first-order method. However, due to the sensitivity to initial conditions, it can be particularly sensitive to setting up initial learning rates at early iterations of the method.

#### 2.4.2 qBang, qBroyden

These methods are inspired by the extension of the classical natural gradient [65] through adaptive techniques [108], introducing both momentum and adaptive learning rates with moving averages, and assuming the approximated QFIM is slowly varying as the parameter space is explored. At each iteration, the metric tensor is characterized by a low-pass filter of learning rate  $\epsilon_i$ , such the inverse Hessian is given by:

$$B_{i+1} = (1 - \epsilon_i)B_i + \epsilon_i \nabla f_i \nabla f_i^{\dagger}. \quad (24)$$

This update leverages Hessian information to update the QFIM [109]. Consequently, the initial approximation of the algorithm dictates the nature of qBang and qBroyden. At the first iteration, one computes either a full or block approximation of the QFIM, followed by an adaptive Broyden method using an averaging window to approximate the QFIM at subsequent optimization steps. At each iteration, the inverse Hessian matrix is given by rank-1 approximation: :

$$B_{i+1}^{-1} = \left( I - \frac{\epsilon_i B_i^{-1} \nabla f_i \nabla f_i^{\dagger}}{1 - \epsilon_i (1 - \nabla f_i^{\dagger} B_i^{-1} \nabla f_i)} \right) \frac{B_i^{-1}}{1 - \epsilon_i} \quad (25)$$

Similarly to the Adam algorithm [110], qBang introduces updates of both variance and momentum, with the variance used to implement a trust region. The incorporation of momentum and moving averages improves stability by shortening unreliable steps. qBroyden, on the other hand, extends a Broyden method (a more general version of BGFS), to the same QFIM approximation without incorporating variance update rules or momentum. It is then a rank-1 approximation of the QFIM using low-pass learning rates and quasi-Newton update rules.

An alternative momentum version of QNG was also introduced in [68], which we will incorporate within this work as a test of the efficacy of adding momentum and sliding averages to QNG-type methods for quantum optimization.

## 2.5 Bayesian optimization for hyperparameters fine-tuning

For the particular case of combinatorial problems involving QAOA the complexity of the objective function implies that sensitivity to optimizer settings will have a substantial impact on the solver's ability to find solutions. In general, hyperparameter fine-tuning of optimizers is a significant challenge in contemporary computer science [111]. In many instances, parameters are selected manually through trial and error by the user, which can be a viable strategy in simple cases but is often time-consuming and ineffective [112]. When the number of parameters is low, and objective function evaluation is computationally expensive, Bayesian optimization presents itself as an ideal candidate, offering a reasonable cost-to-benefit ratio [79].

Bayesian optimization relies on constructing a probabilistic model of the objective function to evaluate the most likely next step to take in order to improve an overall performance metric of interest (see Fig. 1). This method is based on two fundamental concepts: surrogate models and acquisition functions.

#### 2.5.1 Gaussian Processes (GP)

In Bayesian regression models, the distinction is made between parametric and non-parametric models. Parametric models have a finite number of parameters to tune in the regression problem, such as Bayesian linear regression, while non-parametric models can be thought of as an infinite-parameter fit to the objective function. The latter approach can be derived from the former using a kernelization trick. The advantage of this approach lies in its ability to introduce a Gaussian Process (GP), which can integrate both simple and complex data relationships as more data is provided to the model for updating.

A non-parametric Gaussian Process (GP) model, denoted as  $GP(\mu_0, k)$ , is fully characterized by its prior mean function  $\mu_0$  and its positive definite kernel  $K$ . Given a collection of  $n$  measurements, dictated by a set of hyperparameters  $\phi$ , the set of observations  $D_n = \{(\mathbf{x}_i, \mathbf{y}_i)\}_{i=1}^n$ , according to Bayesian inference principles, the random variable  $\mathbb{E}(\mathbf{x})$ , conditioned on the cumulative knowledge of  $D_n$ , follows a normal distribution with the posterior mean and variance:

$$\mu_n(\mathbf{x}) = \mu_0(\mathbf{x}) + \kappa(\mathbf{x})^T (\mathbf{K} + \sigma^2 \mathbf{I})^{-1} (\mathbf{y} - \mathbf{m}) \quad (26)$$

$$\sigma_n^2(\mathbf{x}) = \kappa(\mathbf{x}, \mathbf{x}) - \kappa(\mathbf{x})^T (\mathbf{K} + \sigma^2 \mathbf{I})^{-1} \kappa(\mathbf{x}) \quad (27)$$

where  $\kappa$  represents the vector of covariance terms between point measurements,  $\mathbf{K}$  is the kernel matrix formed from all pairs of  $\kappa$ . A commonly used kernel choice is the Matérn kernel, which belongs to a class of parameterized stationary kernels [113]. We employed this kernel through the automatic fine-tuning feature in `scikit-optimize`.



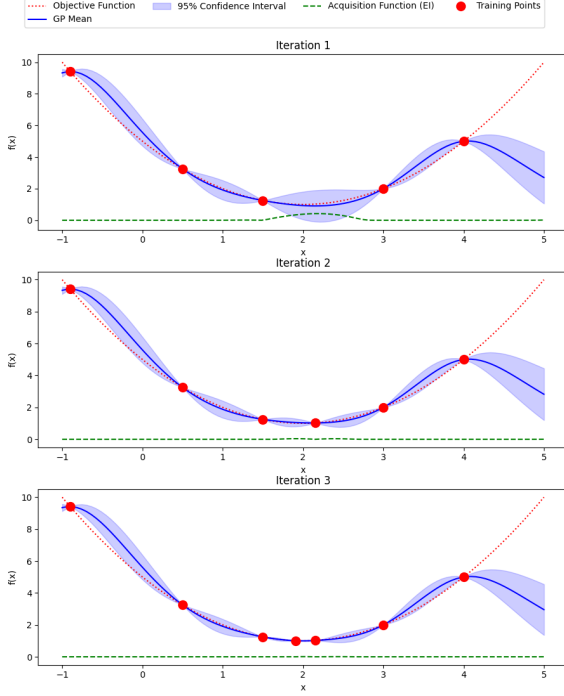


Figure 1: Example of iterative Bayesian process using a Gaussian kernel. Objective function of the form  $f(x) = (x - 2)^2 + 1$ . In practice the objective function is not known, it is only displayed for illustration. Edge acquisition policy and GP + simple Matérn kernel

## 2.5.2 Acquisition function

The second element of Bayesian hyper-parameter estimation involves designing a policy for updating  $\phi$  based on information obtained from the improving surrogate model. Various options are available in the literature regarding such policy, including improvement-based policies [114], optimistic policies [115, 116], and information-based policies, as well as the use of a portfolio of multiple acquisition functions [117]. In this study, we employ the default `gp_hedge` update policy in the `scikit-optimize` function, which is a portfolio that scrambles and randomly selects from lower confidence bound, negative expected improvement, and negative probability of improvement. Utilizing a portfolio-based update policy helps to mitigate biases and leverage the strengths and weaknesses of multiple policies simultaneously [118], making it an appealing choice for benchmarking optimization methods.

## 2.6 Performance benchmarks

The efficacy of the QAOA’s ansatz-optimizer couple is evaluated through a comprehensive assessment of its overall performance capabilities, specifically its ability to provide efficient solutions at reasonable computational costs.

The key metrics employed in this work are explained below.

### 2.6.1 Convergence criteria

As reference point, we solve the synthetic MaxCut problem using a brute force algorithm, and define convergence in terms of the set of solutions that yield an objective function evaluation within a predetermined margin from the optimal solution. This proximity is measured in terms of relative or absolute tolerance. The choice of tolerance typically depends on the scale and specificity of the problem, as well as industry standards. In particular, for logistic problems, including the Traveling Salesman Problem (TSP) and various Vehicle Routing Problems (VRPs), research communities often adhere to established tolerances set by algorithmic competitions and standards. Generally, these tolerances range from 1 to 3 percent for small-scale logistic problems in DIMACS, and 1 to 5 percent for the same types of problems in the ROADEF competition. For large-scale problems, tolerances may be set between 5 and 10 percent for ROADEF and between 3 to 10 percent for DIMACS [119, 120]. In this work, a tolerance of 3% is chosen, and consider a specific run converged if this tolerance is reached at least once.

### 2.6.2 Local Lipschitz constant

In the context of continuous parameter optimization problems, the Lipschitz constant provides a bound on the rate at which a function can change. Specifically, a function  $f : \mathbb{R}^n \rightarrow \mathbb{R}$  is said to be Lipschitz continuous, with a Lipschitz constant  $L$ , if  $L = \sup_{\mathbf{x}, \mathbf{y} \in D, \mathbf{x} \neq \mathbf{y}} \frac{|f(\mathbf{x}) - f(\mathbf{y})|}{\|\mathbf{x} - \mathbf{y}\|}$  for  $D$  in the acceptable parameter model domain. Due to the computational costs involved in precisely calculating the Lipschitz constant, many algorithms instead estimate its value [121, 122]. Rates of convergence of gradient-based methods are bound by the LP constant which sets the optimal step sizes [123], for a given optimization landscape, various gradient based methods can be compared by finding a local bound on the LP constant for a given set of conditions. Equivalently to [123], we focus on approximating  $L$  along optimization “trajectories”, multiple runs creating an overall stochastic form of each methods (multiple starts of the same methods on the same problem, averaged over), computing different  $L$ -metrics as it is shown in the Tab. 2.

By gathering statistics from numerous optimization runs, we aim to observe the difference in behavior between various optimizers when adapting to the landscape geometry, checking the sensitivity to sudden changes and the ability to handle them effectively. Overall, the largest the LP, the smallest the step-size the optimizer need to accept to handle large local variations.

Increasing problem complexity, characterized by high dimensionality and non-convexity, suggests that tightly packed distributions of  $L$  with low median and interquartile range (IQR), coupled with low deviation and aver-

ages, do not necessarily guarantee the best convergence behavior. Rather, a trade-off between speed and accuracy should incorporate well-behaved distributions, where statistical values are commensurate in magnitude. To maximize coverage, employing convergence filtering (i.e., performing all estimations on converged results) necessitates higher averages, accompanied by increased dispersion, albeit with median values tightly clustered around the mean value for optimal performance. Conversely, very stable runs (i.e., non-skewed distributions, low averages, deviations, and IQR) will likely yield strong convergence at low dimensions but may poorly scale due to overfitting or limited adaptivity.

| Metric                    | Interpretation   |
|---------------------------|--|
| Average                   | Low: stable updates in smooth regions, allowing larger step sizes without performance loss or instability.                           |
| Variance                  | Low: consistent and robust across runs, but less adaptable to skewed landscapes. Lower STD enhances predictability upon convergence. |
| Median                    | Low: Frequent low Lipschitz constants indicate stable iterations and effectiveness in less sensitive optimizations.                  |
| Interquartile range (IQR) | Low: clustered Lipschitz constants show consistent performance, suggesting stability in similar landscapes but limited adaptability. |

Table 2: Lipschitz constant statistical metrics used in the benchmark. Very small LP averages indicate low sensitivity, and tendencies to get stuck in local minimas. Target overall for a well behaved optimizer is non-skewed distributions, in most cases,  $IQR > STD$  describes leptokurtic distributions (peaked distributions), when the opposite  $IQR < STD$  can indicate platykurtic distributions (flat distributions) [124]. The LP being a measure of model variation, this means we also desire for optimization purposes rather a peaked distribution, hence a clustered  $IQR > STD$ . Finally, the STD being a measure of overall spread, well-behaved, relatively higher STD is wanted for adaptability of the procedure.

### 2.6.3 Hyperparameters tuning

Exploring the behavior of methods within the hyperparameter space requires a substantial number of function evaluations, grid-division approaches, for example, search for discretized configurations of individual parameters. Using Bayesian optimization, on the other hand, allows for an efficient hyper-parameter space exploration. This approach evaluates what can be expected in terms of overall behavior from each optimizer, even for small numbers of hyperparameters. With Bayesian fine-tuning, one can reasonably expect to observe multiple optimizers converging with parameter selections at least along points of interest, provided that each parameter’s range is defined within practical bounds.

| Methods             | Params       | Desc            |
|---------------------|--------------|-----------------|
| BFGS,DFP,NCG<br>SR1 | $\alpha$     | lr              |
|                     | $\beta$      | ls              |
|                     | $c_1$        | Amijo           |
|                     | $c_2$        | Wolfe           |
| SP-BFGS             | $\alpha$     | lr              |
|                     | $\beta$      | ls              |
|                     | $N_s$        | slope p.        |
|                     | $N_0$        | inter           |
|                     | $c_1$        | Amijo           |
|                     | $c_2$        | wolfe           |
| QNG (block, diag)   | $\alpha$     | lr              |
| qBroyden            | $\alpha$     | lr              |
|                     | $\epsilon$   | filter lr       |
| qBang               | $\alpha$     | lr              |
|                     | $\epsilon$   | filter          |
|                     | $\beta_1$    | decay           |
|                     | $\beta_2$    | decay           |
| m-QNG               | $\alpha$     | lr              |
|                     | $\epsilon$   | filter lr       |
|                     | $\beta_1$    | decay           |
|                     | $\beta_2$    | decay           |
| SPSA                | $\alpha$     | decay lr        |
|                     | $a_{init}$   | init lr         |
|                     | $c_{init}$   | init pert       |
|                     | $\gamma$     | decay pert      |
|                     | $A$          | amplitude decay |
| 2SPSA               | $\alpha$     | decay lr        |
|                     | $a_{init}$   | init lr         |
|                     | $c_{init}$   | init pert       |
|                     | $a_{init}^H$ | init lr         |
|                     | $c_{init}^H$ | init pert       |
|                     | $\gamma$     | decay pert      |
| QNPSA               | $\alpha$     | lr              |
|                     | $\epsilon$   | amplitude decay |
|                     | $\gamma$     | decay           |

Table 3: The following hyperparameters are selected for tuning on each method: Amijo and Wolfe’s line backtracking algorithm parameters, which include curvature and improvement; ls, denoting the line search penalty term associated with the learning rate update; perturbations of SPSA type, referred to as pert; and lr, representing any learning rate. Additionally, the exponent  $H$  represents an approximation of the Hessian matrix.

An overview of the hyper-parameter space per method is presented in Tab.3, while additional information about the selected search space for each parameter is provided in App.C.

## 3 Results

First, we conducted a series of exploratory runs for each optimizer on weighted graphs with 3 and 5 nodes, ad-

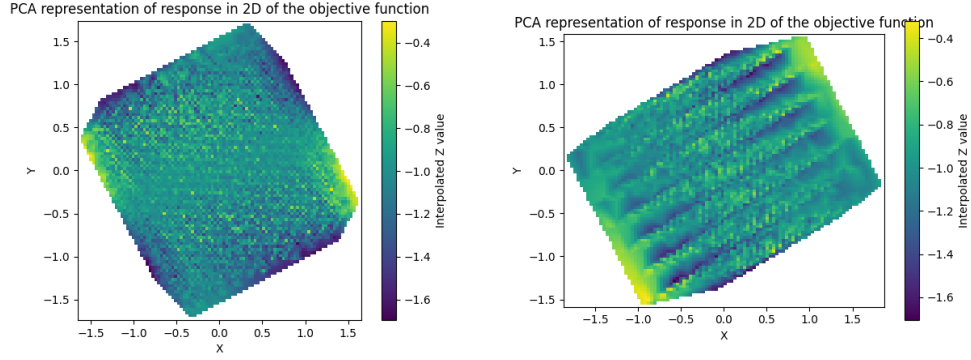


Figure 2: 3 nodes problem (left) and 7 node problem (right) PCA analysis in a grid exploration. Increasing the problem size drastically increases rugosity and local minima, central symmetry due to symmetries in parametrization of Pauli gates.

addressing the MaxCut problems using a one-layer QAOA ansatz (as detailed in Sec.B). The initial conditions were fully randomized but can be reproduced through the seed settings. We first present a high-dimensional function visualization, utilizing Principal Component Analysis (PCA) and a random projection onto a lower-dimensional plane. This illustrates the highly complex structures of the parameter space, characterized by non-convexities that scale with problem dimensions. We also performed an initial Bayesian hyperparameter estimation to identify a well-suited parameter set, as shown in Tab.3.

Subsequently, we present three benchmarks: Firstly, a small benchmark involving 3 nodes to assess convergence robustness by analyzing local Lipschitz constants discussed in Sec.2.6.2, followed by an examination of convergence behavior. Secondly, we conducted a benchmark with a larger set of properties through multiple Bayesian sweeps, as described in Sec.2.6.3. This latter benchmark was explored by gathering statistics on the averaged behaviors across various optimization initial conditions, allowing for a systematic discussion of what users can expect from these different optimization methods.

### 3.1 Landscape analysis

To motivate the following discussion, we investigate the optimization landscape of the QAOA ansatz using Principal Component Analysis (PCA) [125] in Fig. 2. This validates previous observations that, in shallow PQC, the geometric features of the optimization landscape degrade with increasing dimensions [32]. Low-dimensional problems exhibit highly textured surfaces with clearly defined lower and upper regions. However, in the 7-node problem, we observe the emergence of repeated valleys and peaks, leading to more intricate structures and potential local minima.

An interesting technique for visualizing high-dimensional functions involves projecting higher-dimensional objects into random lower-dimensional constructs, which

preserves distances from the original high-dimensional space [126]. In this case, we proceed by picking two random directions in parameter space in a 5 qubit ansatz solving the 5 nodes standard problem (Sec. B). We set a 300 steps from  $[-1, 1]$  and explore the parameter space along multiple random directions. This method shows even in shallow QAOA complex interference patterns and hyperbolic structures Fig. 3. Those figures represent a visual motivation for natural gradient methods: we see that in parameter space, a more suited metric, i.e. the Fubini-Study metric tensor, which describes a Riemannian geometry Eq. (20).

### 3.2 Convergence analysis

**Convergence robustness** is assessed by compiling results from runs on the same 3-node regular graph MaxCut problem, initiated from a random set of initial points. In these evaluations, we exclude non-converging runs, defined as those that do not achieve a 1% tolerance, to better highlight the overall convergence behavior. The stopping condition at 1% allows us to observe the dynamic behavior of the methods while ensuring that there is no influence from stagnated trajectories in local minima or excessive iterations. Thus, the Lipschitz property (LP) serves as an effective descriptor of how the methods adapt to the same objective function geometry. To avoid statistical biases, we only consider experiments where at least 50% of the runs achieved the specified tolerance. We present four statistical metrics representing the LP estimation for the given problem in Sec. 2.6.2.

Raw results in Tab. 4 shows natural gradient and quasi-Newton methods have significantly different LP estimations. On average, natural gradients provide much higher LP estimations, this means that the natural gradient preconditioning technically allows for larger step size, this validates of why natural gradients are introduced in the first place: providing preconditioning from the true direction of greater change in the optimization space according to information geometry. This is expected from

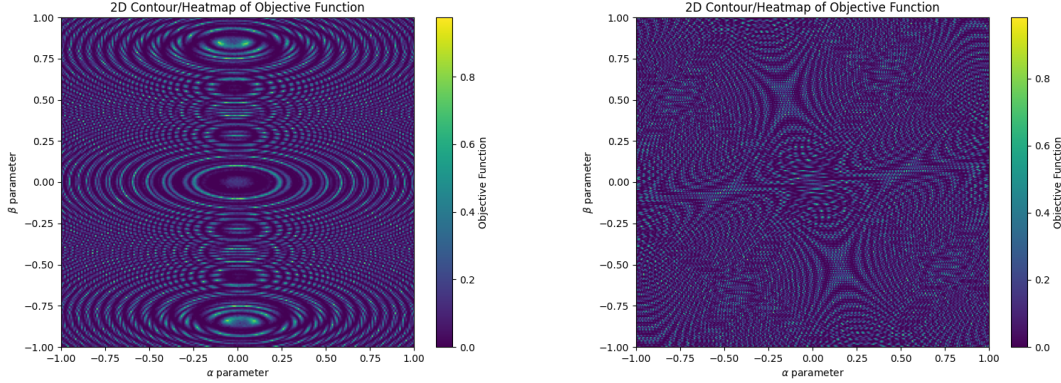


Figure 3: For 300 grid discretization, examples of two randomly picked directions in 5 nodes problem App. B, defining two random parameterized lines. Two random directions define a plan in the hyper-space in which the objective function is defined, parameters  $\alpha$  and  $\beta$  are unique parameterization of each random lines.

| Methods     | av             | std     | med            | iqr          |
|-------------|----------------|---------|----------------|--------------|
| BFGS        | 10.736         | 18.855  | 3.353          | 7.737        |
| SR1         | 12.0144        | 19.190  | 4.055          | 7.564        |
| NCG         | 60.643         | 116.662 | 2.679          | 31.514       |
| SP-BFGS     | 90.571         | 43.590  | 95.860         | <b>51.84</b> |
| DFP         | <b>93.568</b>  | 30.862  | <b>103.362</b> | 33.448       |
| QNG (diag)  | 221.578        | 66.464  | 210.936        | 77.135       |
| QNG (block) | 404.684        | 119.77  | 381.91         | 129.793      |
| qBroyden    | 411.238        | 138.408 | 386.249        | 149.343      |
| qBang       | 232.709        | 74.829  | 217.482        | 61.351       |
| m-QNG       | <b>632.674</b> | 150.492 | 611.474        | 191.993      |

Table 4: LP constant estimation for each method with full gradient estimation, 3 nodes, Bayesian defaults in Tab. 5, 1000 experiments per method. seed=32, 20 max iterations

the definition of the natural gradient, which indicates the true gradient in the quantum parametric space. High average LP means rapid convergence, Tab. 4 shows that SP-BFGS and DFP dominate quasi-Newton methods, where m-QNG and qBroyden show the stronger convergence. Those raw points however, do not show the full picture. Fig. 4 represents normalized distributions of the LP estimations on the mean. As explained on distribution in Sec. 2.6.2, BFGS, SR1 and NCG show very skewed distributions: they are not well behaved in addition to provide slower convergence than the two other quasi-Newton methods. Tab. 2 helps interpreting the data: the methods to the left are -as seen by the optimizers- behaving as flat landscape, provide poor convergence and due to low median provide low sensitivity to updates. The latter is not a sought after feature for non-convex geometries, complex geometries require high exploration. Furthermore DFP and SP-BFGS provides well rounded, regular and peaked distributions, with the only difference being a slightly higher scaling for SP-BFGS with slightly lower median, indicating slightly more rigid updates for SP-BFGS, but with more exploration and dispersion at each runs. Overall, natural gradient methods provide sim-

ilar performances against each other, to the exception to m-QNG showing the lower variation overall.

These results demonstrate the behavior under ideal conditions, characterized by the lowest geometric complexity, as the 3-node system represents the simplest dimensional problem for MaxCut, using the most shallow QAOA ansatz. The remainder of this analysis will examine varying behaviors as we scale up the problems.

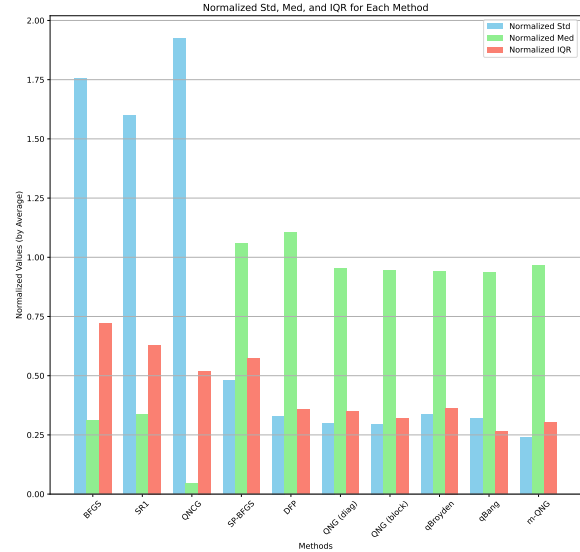


Figure 4: Each method normalized on their averages. We find three families of convergence behaviors: first are the skewed distributions: BFGS, SR1 and NCG. Well-behaved leptokurtic distributions (peaked) with SP-BFGS, DFP, QNG(block and diagonal), qBroyden and m-QNG. Last behavior are platykurtic distributions (flat) with qBang.

**Convergence behavior** can be investigated through an evaluation of convergence trajectories. While the previous paragraph offers a geometric perspective on a specific problem, it does not provide insights into how the methods perform as the complexity of the objective function increases, specifically with larger parameter spaces and higher dimensionality. Sequentially we investigate quasi-Newton preconditioners, natural gradient based methods, then we give some comments about the introduction of second order estimation in stochastic methods.

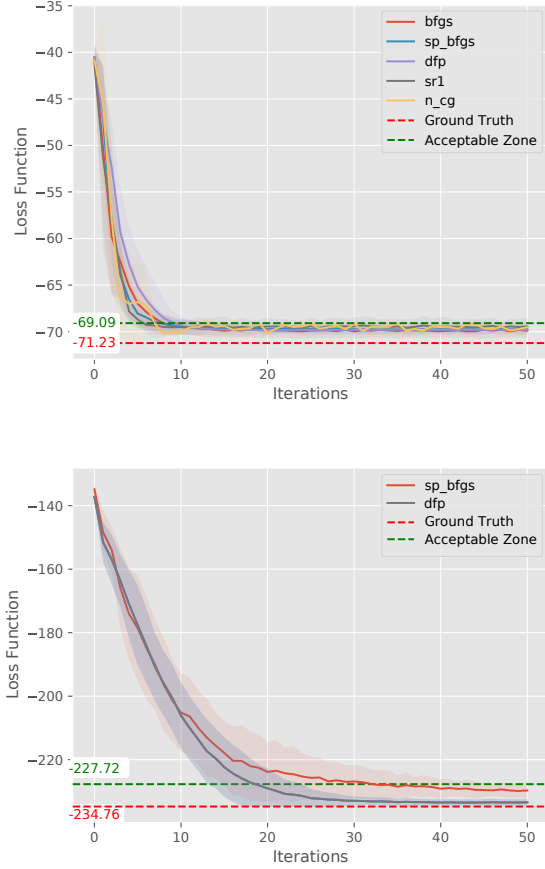


Figure 5: Convergence analysis, quasi-Newton types methods for benchmark problem, *top* figure problem with 3 nodes, *low* figure problem with 5 nodes of seed=32, 50 experiments over randomly sampled initial conditions. 512 shots, 60 iterations

**Discussion** The classic preconditioners SR1 and BFGS and NCG seems from Fig. 5 and Tab. 4 to be entirely unsuitable for a QAOA solver applied to Max-Cut. They exhibit low average LP values, suggesting slow convergence overall, and demonstrate a null convergence ratio at 3% tolerance for 5-node problems. In contrast, DFP and SP-BFGS present superior characteristics, offer-

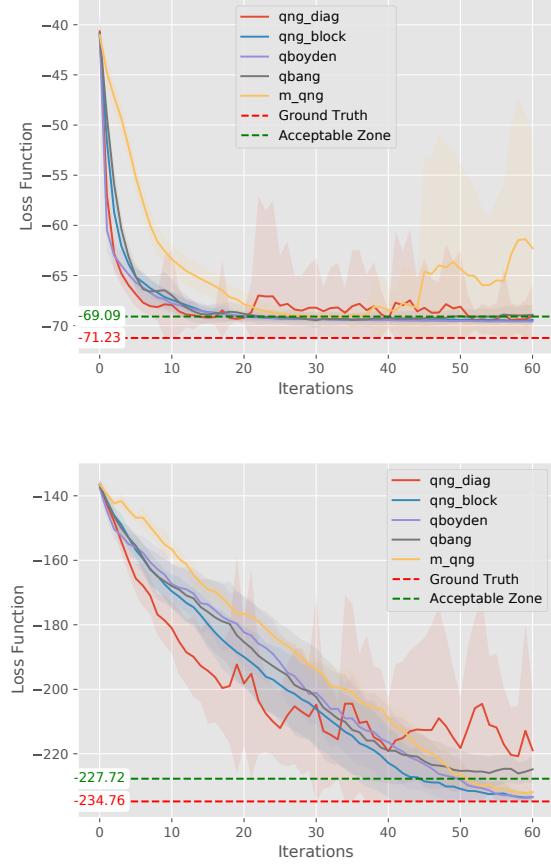


Figure 6: Convergence analysis, QNG types methods for benchmark problem, *top* figure problem with 3 nodes, *low* figure problem with 5 nodes of seed=32, 50 experiments over randomly sampled initial conditions. 512 shots, 60 iterations

ing quality solutions, strong convergence, and a favorable trade-off for exploring the parameter space.

On the side of the natural gradient experiments, although natural gradient promises better robustness in Tab. 4, Fig. 6, demonstrate that this does not necessarily translate to improved performance in practice. This is likely due to the QNG algorithms suffering from additional statistical noise in the QFIM matrix evaluation. This seems to remain true regardless of the QFIM approximation choice however, as qBang and qBroyden rely on approximations of the QFIM through a learned filter and moving average.

Finally, in Fig. 7, we compare performances between the 3-node and 5-node configurations. We observe significant improvements for QNSPSA and 2SPSA at 3 nodes, though this comes with increased statistical variations across runs. However, at 5 nodes, the translation of hyperparameters from the 3-node case fails to maintain consistency in capturing second-order information. This sug-



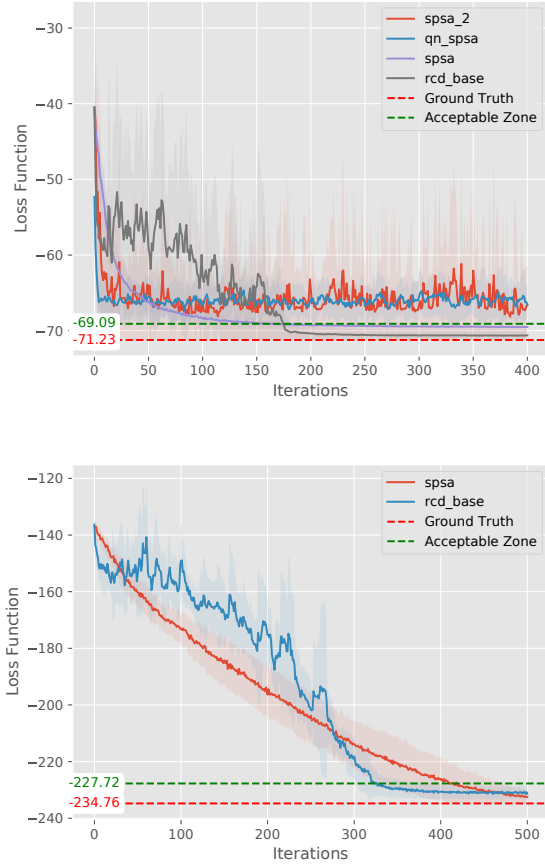


Figure 7: Convergence analysis, stochastic methods types methods for benchmark problem, *top* figure problem with 3 nodes, *low* figure problem with 5 nodes of seed=32, 50 experiments over randomly sampled initial conditions. 512 shots, 400 max iterations

gests that retuning is likely necessary for second-order stochastic methods, even with minor changes in problem dimensions and parameters.

In the next section, we go into more details and explore the full capabilities of those optimizers through the exploration of their hyperparameter space using Bayesian optimization, allowing for an in-depth cost to performance analysis.

### 3.3 Benchmarks

In this section, we explore significant results from overall benchmarks in appendix App. C.1, highlighting specific sections providing commentary. During those runs made on a 10-CPU node we provide two bayesian sweeps for each optimizer through all test problems in Sec. B from 3 nodes to 8 nodes. The first sweep is set without stopping condition to maximum iteration, the second with

stopping condition at 3% tolerance. Measure falls into performance and cost metrics such as last objective function value, walltime(s), Hamming distance to solution (binary distance from true binary solution), convergence ratio, Calls to QPU (qCalls), and with exit condition to convergence: average time per iteration, average qCall, qCall per iteration, average iteration to convergence

The averaged objective function with and without exit condition are used as cost function of the Bayesian search. In the following results, each points should be interpreted as an averaged value over 20 runs with initial conditions picked randomly from an uniform distribution. we note that NCG is absent to computation over 3 nodes, as the method fails to converge further at all. This is most likely due to the fact that CG-type methods perform best in locally-convex geometries, which is not the case for Max-Cut QAOA as shown in Sec. 3.1.

**Performances** By incrementally increasing the problem size and constructing convex-hull graphs, we can expand upon previous observations regarding the full expressible behavior set of the optimizers. The shapes of these graphs define the boundaries within a specifically chosen behavior space. Optimizers that share the same surface area on the graph across multiple metrics should be expected to perform similarly on a given QAOA Max-Cut problem.

In Fig. 8 representing 3 and 5 nodes problems, we observe the failure of BFGS, NCG and SR1 methods to adapt to the optimization landscape as it scales. Already for 3 nodes, only DFP and SP-BFGS find hyper-parameter set with 100% runs converging to 3%. Furthermore, DFP allows for better scaling reaching close to 100% convergence, this trend is validated up to 8 nodes in Fig. 25.

Scaling again from 3 nodes to 5 nodes shows a rapid loss of convergence ratios for qBroyen in Fig. 9, showing poor performances compared to the other methods. One can see however that qBang and qBroyden methods provide significantly faster operations for similar performances, depending on initial conditions.

Introducing secant penalization facilitates a significantly lower cost while maintaining a useful convergence ratio. The average improvements associated with this approach increase with problem size, as illustrated in Fig. 10.

**Cost analysis** The cost analysis is done through a similar procedure, with added a with a 3% stopping condition, hence measuring cost metrics to convergence. To reach tolerance, we observe validating trends concerning SP-BFGS capabilities in finding quality solutions for less resources in time and QPU queries in Fig. 11. Those trends are validated by scaling further the tests up to 8 nodes in App. C.1. In normal use, observations on poor convergence quality for SR1, NCG and BFGS from 3 nodes problem to 5 nodes problem in Fig. 11 shows complete failure in finding optimal solutions. On the other hand, SP-BFGS provides significantly better cost per iteration than even

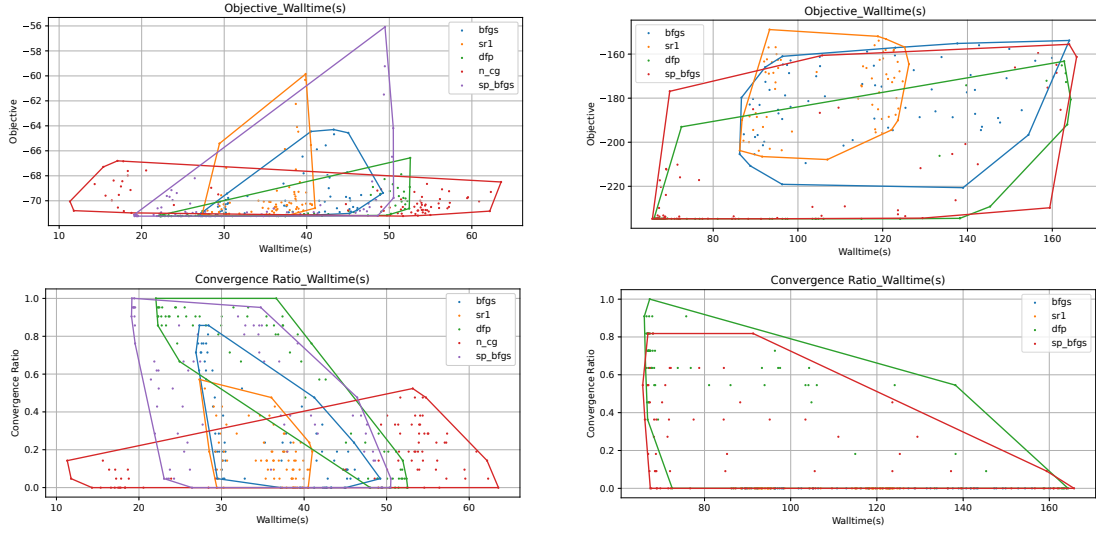


Figure 8: 3 nodes problem (left) and 5 nodes problem (right) on the quasi-Newton methods, 70 bayesian sweeps on second order methods, stopping condition reached at maxit 60 iterations. Objective function are last objective values (averaged over 20 runs), Convergence ratio is the ratio of runs arriving to 3% tolerance (20 runs), walltime (s) is measured from call of first iteration to stopping condition reached.

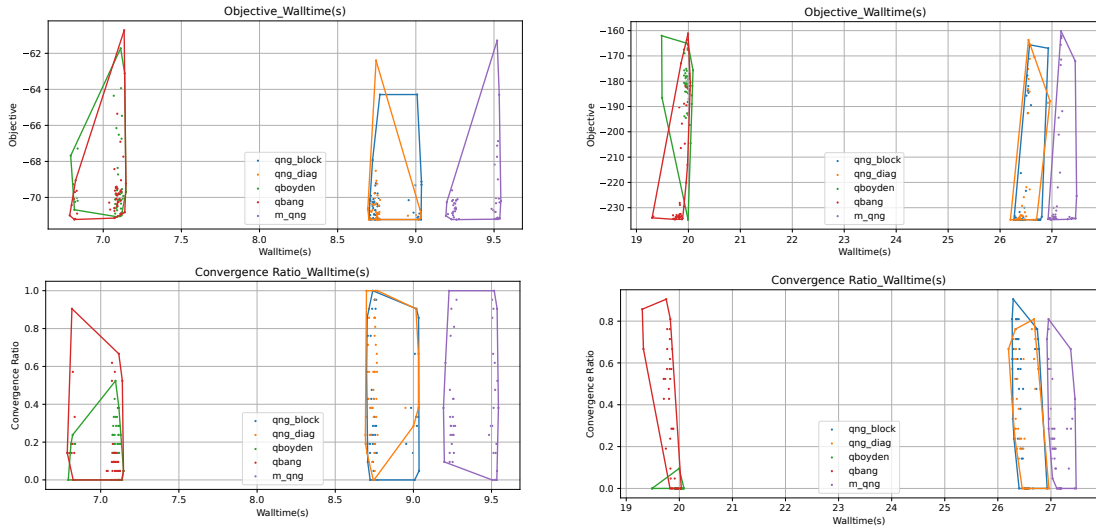


Figure 9: 3 nodes problem (left) and 5 nodes problem (right), 70 bayesian sweeps Natural gradient methods, stopping condition reached at maxit 60 iterations. Objective function are last objective values (averaged over 20 runs), Convergence ratio is the ratio of runs arriving to 3% tolerance (20 runs), walltime (s) is measured from call of first iteration to stopping condition reached.

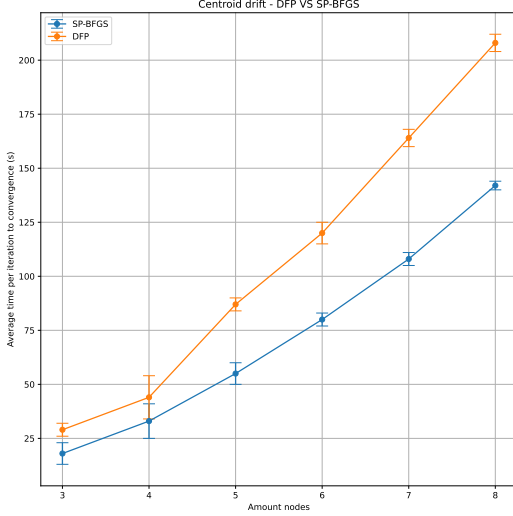


Figure 10: Distance between SP-BFGS and DFP centroids in time per iterations to convergence. We observe from a well-behaved quasi-Newton methods such as DFP form a secant-penalized update, the performance gain in time per iteration is increasing with the problem size.

DFP. This is not only true for overall walltime, but also the average quantum calls to convergence still in Fig. 11.

The improvement in generalization and cost for SP-BFGS is likely attributable to the secant-penalization mechanism, which updates the Hessian matrix only when sufficient information is gathered from sampling the objective function. The cost advantage from DFP to SP-BFGS appears to increase as the problem dimension grows; this can be confirmed by examining Fig. 10, which illustrates the differences in centroid distances and time per iteration (to convergence) between DFP and SP-BFGS. Overall, these figures indicate that DFP is the best-performing quasi-Newton method; however, there are hyperparameter configurations in which SP-BFGS significantly outperforms DFP in terms of execution time.

Introducing the secant-penalization allows for a significantly lower cost while keeping useful convergence ratio, whose average improvements increases with the problem size Fig.10

At convergence, qBang qBang is significantly more cost-effective in terms of quantum calls compared to QNG methods, resulting in a drastic reduction in average time per iteration. The introduction of momentum in QNG pushes this convergence speed from QNG (block or diagonal approximation of the QFIM) to the same convergence speed than qBang. Note that convergence speed per iteration allows to compare overall behavior: QNG provide stronger convergence, but at the cost of the block

matrix QFIM estimation, which qBroyden and qBang are avoiding. This result however do show experimentally that qBang approximates the QFIM through a learned parametric filter over the optimization history. At scale however to 8 nodes, QNG block and diagonal only remain capable of producing 3% solutions App. C.1.

### 3.4 Second order information in stochastic methods

Introducing second-order estimation in SPSA necessitates additional hyperparameters that must be fine-tuned for optimal performance. The quality of the second-order information estimation is contingent upon these parameters, which must either be pre-tuned or leveraged from past experiences. Overall, we see the first advantage of first order stochastic methods is to provide solutions at constant speed in Fig.13 again from 3 nodes to 5 nodes, which shows increase difficulty in fine-tuning parameters. QN-SPSA however provides an improvement on SPSA2 at 400 iterations, at the cost of more QPU calls C.1.

Overall, QNSPSA significantly outperforms SPSA2, particularly due to its advantage of having fewer hyperparameters to tune, which allows for more efficient use of second-order information compared to SPSA2. However, for the chosen parameters, second-order methods such as SPSA and RCD, especially SPSA, still provide the last non-zero convergence ratios for larger problems, as detailed in App. C.1. In practice, both QNSPSA and SPSA2 should only be utilized when the statistical error on samples can be minimized, for instance, through high shot counts, to facilitate an unbiased estimation of the Hessian or QFIM.

## 4 Conclusion

In this paper, we demonstrated that the choice of preconditioner in second-order methods significantly influences optimization outcomes in shallow QAOA ansatz. The complex structure of the optimization landscape of the PQC objective function led us to conclude that SR1, BFGS, and NCG are unsuitable for these types of problems. In contrast, the DFP method exhibits the best performance in this context.

Our contribution introduces a simple secant-penalization rule that stabilizes BFGS when confronted with non-convexities and noisy gradient sampling. Notably, SP-BFGS is less computationally expensive in terms of QPU calls and overall computational time compared to DFP, which we identified as the best-behaved quasi-Newton preconditioner. Furthermore, the tuning of the additional phenomenological parameters ( $N_0, N_1$ ) does not present significant challenges.

Additionally, we found that for small dimensions, QNG-type methods provide much faster convergence than second-order methods, albeit at a higher cost due to QFIM estimation. Although more economical methods like qBang and qBroyden still offer faster conver-



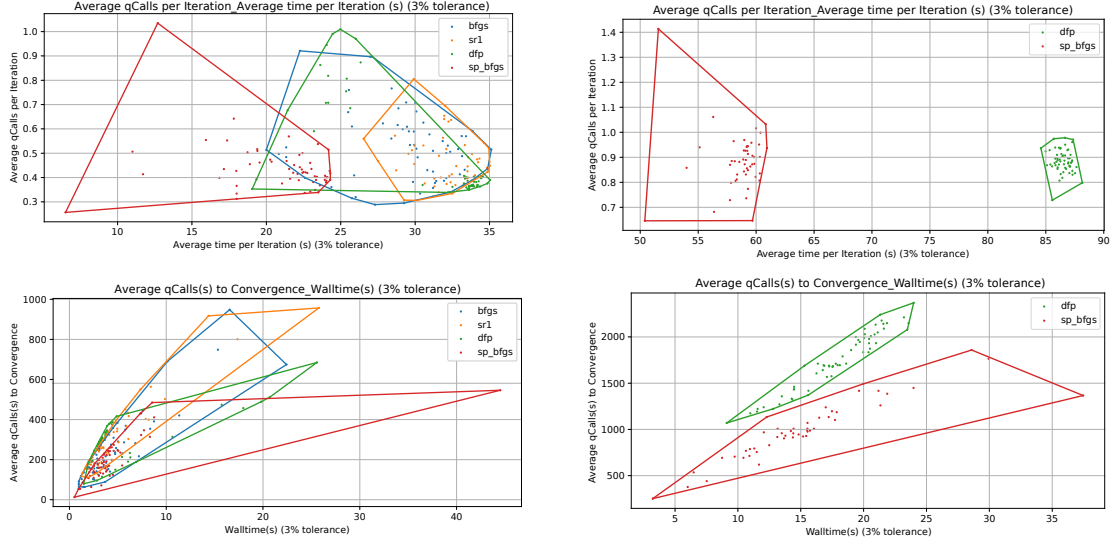


Figure 11: 3 nodes problem (left) and 5 nodes problem (right), 70 bayesian sweeps on second order methods, stopping condition reached when 3% tolerance is reached. Objective function are last objective values (averaged over 20 runs), Convergence ratio is the ratio of runs arriving to 3% tolerance (20 runs), walltime (s) is measured from call of first iteration to stopping condition reached.

gence than quasi-Newton methods, their QFIM approximations—based on a learned mechanism over the optimization history—tend to degrade as the complexity of the landscape increases.

Finally, incorporating second-order information in stochastic problems necessitates careful tuning of hyperparameters, without guaranteeing improvements over first-order methods such as SPSA or RCD. While QNSPSA outperforms SPSA2, it is likely to require a high shot count to prevent the QFIM statistical estimator from becoming counterproductive.

Future research should focus on integrating a secant-penalization rule into the QFIM estimation of qBang to bypass uninformative gradient measurements during optimization and avoid cumulative errors. Additionally, further investigation into the penalization rule within SP-BFGS is warranted. We demonstrated that a simple linear model with an interception rule was sufficient to enhance preconditioner behavior; however, more sophisticated rules, problem-specific schedules, phenomenological models, or machine learning approaches could be introduced in Eq. 16, with their formulation depending on the uniform gradient bounded noise hypothesis.

## 5 Acknowledgements

This research was made possible by the financing of the BMWK-Project »EniQmA« for the Systematic Development of Hybrid Quantum Computing Applications.

## 5.1 References and footnotes

### References

- [1] Edward Farhi and Aram W Harrow. Quantum supremacy through the quantum approximate optimization algorithm, 2019.
- [2] Manuel S. Rudolph, Jacob Miller, Danial Motlagh, Jing Chen, Atithi Acharya, and Alejandro Perdomo-Ortiz. Synergistic pretraining of parametrized quantum circuits via tensor networks. *Nature Communications*, 14(1), 2023.
- [3] Marcello Benedetti, Erika Lloyd, Stefan Sack, and Mattia Fiorentini. Parameterized quantum circuits as machine learning models. *Quantum Science and Technology*, 4(4):043001, 2019.
- [4] Zhan Yu, Qiu hao Chen, Yuling Jiao, Yinan Li, Xiliang Lu, Xin Wang, and Jerry Zhijian Yang. Provable advantage of parameterized quantum circuit in function approximation, 2023.
- [5] M. Cerezo, Andrew Arrasmith, Ryan Babbush, Simon C. Benjamin, Suguru Endo, Keisuke Fujii, Jarrod R. McClean, Kosuke Mitarai, Xiao Yuan, Lukasz Cincio, and Patrick J. Coles. Variational quantum algorithms. *Nature Reviews Physics*, 3(9):625–644, 2021.
- [6] Sam McArdle, Suguru Endo, Alán Aspuru-Guzik, Simon C. Benjamin, and Xiao Yuan. Quantum computational chemistry. *Reviews of Modern Physics*, 92(1), 2020.

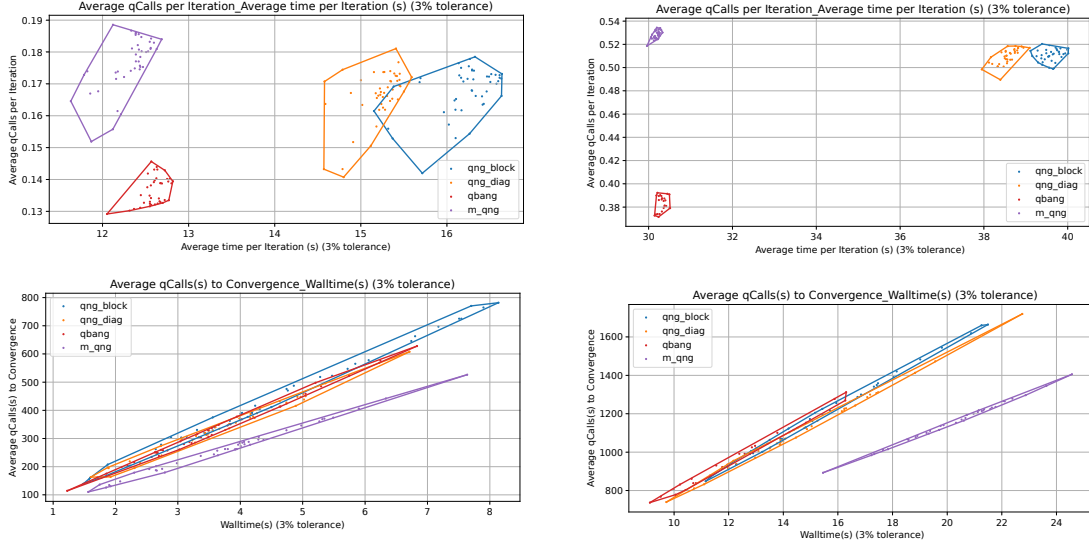


Figure 12: 3 nodes problem (left) and 5 nodes problem (right), 70 bayesian sweeps on natural gradient methods, stopping condition reached when 3% tolerance is reached. Objective function are last objective values (averaged over 20 runs), Convergence ratio is the ratio of runs arriving to 3% tolerance (20 runs), walltime (s) is measured from call of first iteration to stopping condition reached.

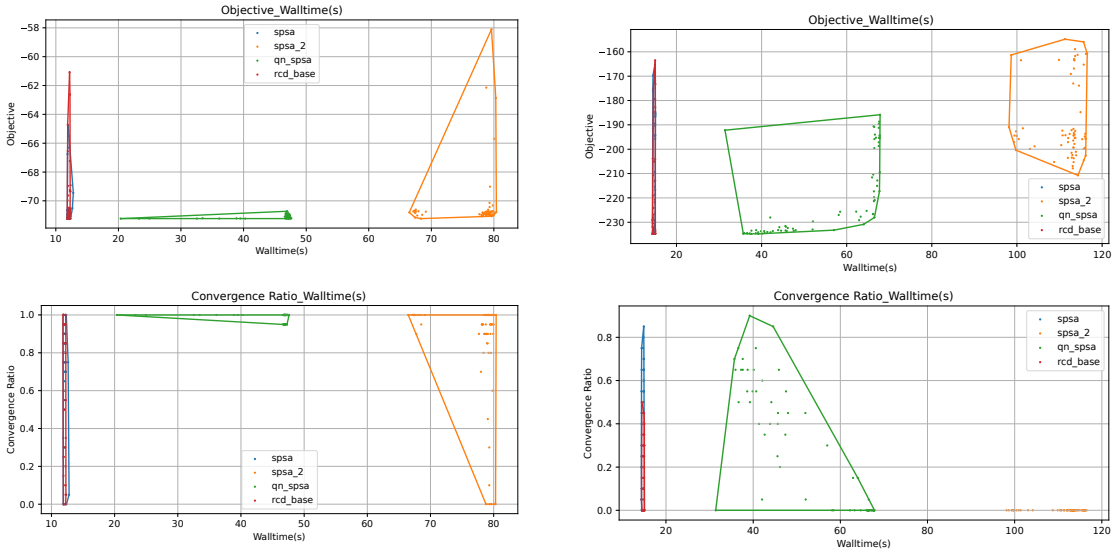


Figure 13: 3 nodes problem (left) and 5 nodes problem (right), 70 bayesian sweeps on stochastic methods, stopping condition reached when 400 max iteration is reached. Objective function are last objective values (averaged over 20 runs), Convergence ratio is the ratio of runs arriving to 3% tolerance (20 runs), walltime (s) is measured from call of first iteration to stopping condition reached.

- [7] Shaojun Guo, Jinzhao Sun, Haoran Qian, Ming Gong, Yukun Zhang, Fusheng Chen, Yangsen Ye, Yulin Wu, Sirui Cao, Kun Liu, Chen Zha, Chong Ying, Qingling Zhu, He-Liang Huang, Youwei Zhao, Shaowei Li, Shiyu Wang, Jiale Yu, Daojin Fan, Dachao Wu, Hong Su, Hui Deng, Hao Rong, Yuan Li, Kaili Zhang, Tung-Hsun Chung, Futian Liang, Jin Lin, Yu Xu, Lihua Sun, Cheng Guo, Na Li, Yong-Heng Huo, Cheng-Zhi Peng, Chao-Yang Lu, Xiao Yuan, Xiaobo Zhu, and Jian-Wei Pan. Experimental quantum computational chemistry with optimized unitary coupled cluster ansatz. *Nature Physics*, 2024.
- [8] Hongbin Liu, Guang Hao Low, Damian S. Steiger, Thomas Häner, Markus Reiher, and Matthias Troyer. Prospects of quantum computing for molecular sciences. *Materials Theory*, 6(1), 2022.
- [9] Alberto Peruzzo, Jarrod McClean, Peter Shadbolt, Man-Hong Yung, Xiao-Qi Zhou, Peter J. Love, Alán Aspuru-Guzik, and Jeremy L. O’Brien. A variational eigenvalue solver on a photonic quantum processor. *Nature Communications*, 5(1), 2014.
- [10] Niklas Pirnay, Vincent Quentin Ulitzsch, Frederik Wilde, Jens Eisert, and Jean-Pierre Seifert. An in-principle super-polynomial quantum advantage for approximating combinatorial optimization problems via computational learning theory. *Science advances*, 10 11:eadj5170, 2022.
- [11] Edward Farhi, Jeffrey Goldstone, and Sam Gutmann. A quantum approximate optimization algorithm, 2014.
- [12] Edward Farhi, Jeffrey Goldstone, Sam Gutmann, and Michael Sipser. Quantum computation by adiabatic evolution, 2000.
- [13] Amira Abbas, Andris Ambainis, Brandon Augustino, Andreas Bärttschi, Harry Buhrman, Carleton Coffrin, Giorgio Cortiana, Vedran Dunjko, Daniel J. Egger, Bruce G. Elmegreen, Nicola Franco, Filippo Fratini, Bryce Fuller, Julien Gacon, Constantin Gonciulea, Sander Gribling, Swati Gupta, Stuart Hadfield, Raoul Heese, Gerhard Kircher, Thomas Kleinert, Thorsten Koch, Georgios Korpas, Steve Lenk, Jakub Marecek, Vanio Markov, Guglielmo Mazzola, Stefano Mensa, Naeimeh Mohseni, Giacomo Nannicini, Corey O’Meara, Elena Peña Tapia, Sebastian Pokutta, Manuel Proissl, Patrick Rebentrost, Emre Sahin, Benjamin C. B. Symons, Sabine Törnøw, Victor Valls, Stefan Woerner, Mira L. Wolf-Bauwens, Jon Yard, Sheir Yarkoni, Dirk Zechiel, Sergiy Zhuk, and Christa Zoufal. Quantum optimization: Potential, challenges, and the path forward, 2023.
- [14] Richard P. Feynman. Simulating physics with computers. *International Journal of Theoretical Physics*, 1982.
- [15] Benedikt Fauseweh. Quantum many-body simulations on digital quantum computers: State-of-the-art and future challenges. *Nature Communications*, 15, 03 2024.
- [16] I.M. Georgescu, S. Ashhab, and Franco Nori. Quantum simulation. *Reviews of Modern Physics*, 86(1):153–185, 2014.
- [17] Alexandre Choquette, Agustin Di Paolo, Panagiotis Kl. Barkoutsos, David Sénéchal, Ivano Tavernelli, and Alexandre Blais. Quantum-optimal-control-inspired ansatz for variational quantum algorithms. *Physical Review Research*, 3(2), 2021.
- [18] D.J. Egger and F.K. Wilhelm. Adaptive hybrid optimal quantum control for imprecisely characterized systems. *Physical Review Letters*, 112(24), 2014.
- [19] Alicia B. Magann, Christian Arenz, Matthew D. Grace, Tak-San Ho, Robert L. Kosut, Jarrod R. McClean, Herschel A. Rabitz, and Mohan Sarovar. From pulses to circuits and back again: A quantum optimal control perspective on variational quantum algorithms. *PRX Quantum*, 2:010101, Jan 2021.
- [20] Christa Zoufal, Aurélien Lucchi, and Stefan Woerner. Quantum generative adversarial networks for learning and loading random distributions. *npj Quantum Information*, 5(1), 2019.
- [21] Amira Abbas, David Sutter, Christa Zoufal, Aurélien Lucchi, Alessio Figalli, and Stefan Woerner. The power of quantum neural networks. *Nature Computational Science*, 1(6):403–409, 2021.
- [22] Carlos Bravo-Prieto, Ryan LaRose, M. Cerezo, Yigit Subasi, Lukasz Cincio, and Patrick J. Coles. Variational quantum linear solver. *Quantum*, 7:1188, 2023.
- [23] Samson Wang, Enrico Fontana, M. Cerezo, Kunal Sharma, Akira Sone, Lukasz Cincio, and Patrick J. Coles. Noise-induced barren plateaus in variational quantum algorithms. *Nature Communications*, 12(1), 2021.
- [24] M. Cerezo, Akira Sone, Tyler Volkoff, Lukasz Cincio, and Patrick J. Coles. Cost function dependent barren plateaus in shallow parametrized quantum circuits. *Nature Communications*, 12(1), 2021.
- [25] Zoë Holmes, Kunal Sharma, M. Cerezo, and Patrick J. Coles. Connecting ansatz expressibility to gradient magnitudes and barren plateaus. *PRX Quantum*, 3:010313, Jan 2022.
- [26] Jarrod R. McClean, Sergio Boixo, Vadim N. Smelyanskiy, Ryan Babbush, and Hartmut Neven. Barren plateaus in quantum neural network training landscapes. *Nature Communications*, 9(1), 2018.
- [27] Alistair Letcher, Stefan Woerner, and Christa Zoufal. Tight and efficient gradient bounds for parameterized quantum circuits, 2024.

- [28] Antonio Anna Mele, Armando Angrisani, Soumik Ghosh, Sumeet Khatri, Jens Eisert, Daniel Stilck França, and Yihui Quek. Noise-induced shallow circuits and absence of barren plateaus, 2024.
- [29] Kunal Sharma, M. Cerezo, Lukasz Cincio, and Patrick J. Coles. Trainability of dissipative perceptron-based quantum neural networks. *Phys. Rev. Lett.*, 128:180505, May 2022.
- [30] Arthur Pesah, M. Cerezo, Samson Wang, Tyler Volkoff, Andrew T. Sornborger, and Patrick J. Coles. Absence of barren plateaus in quantum convolutional neural networks. *Physical Review X*, 11(4), 2021.
- [31] Martin Larocca, Piotr Czarnik, Kunal Sharma, Gopikrishnan Muraleedharan, Patrick J. Coles, and M. Cerezo. Diagnosing barren plateaus with tools from quantum optimal control. *Quantum*, 6:824, 2022.
- [32] Patrick Huembeli and Alexandre Dauphin. Characterizing the loss landscape of variational quantum circuits. *Quantum Science and Technology*, 6(2):025011, 2021.
- [33] Ruslan Shaydulin, Ilya Safro, and Jeffrey Larson. Multistart methods for quantum approximate optimization. In *2019 IEEE High Performance Extreme Computing Conference (HPEC)*. IEEE, September 2019.
- [34] John Preskill. Quantum computing in the nisq era and beyond. *Quantum*, 2:79, August 2018.
- [35] Emilie Chouzenoux, Jean-Baptiste Fest, and Audrey Repetti. A kurdyka-lojasiewicz property for stochastic optimization algorithms in a non-convex setting, 2023.
- [36] Prateek Jain and Purushottam Kar. Non-convex optimization for machine learning. *Foundations and Trends® in Machine Learning*, 10(3–4):142–336, 2017.
- [37] Soham De, Anirbit Mukherjee, and Enayat Ullah. Convergence guarantees for rmsprop and adam in non-convex optimization and an empirical comparison to nesterov acceleration, 2018.
- [38] J. Gidi, B. Candia, A. D. Muñoz-Moller, A. Rojas, L. Pereira, M. Muñoz, L. Zambrano, and A. Delgado. Stochastic optimization algorithms for quantum applications, 2023.
- [39] James C. Spall. A stochastic approximation technique for generating maximum likelihood parameter estimates. In *1987 American Control Conference*, pages 1161–1167, 1987.
- [40] James C. Spall. A one-measurement form of simultaneous perturbation stochastic approximation. *Automatica*, 33(1):109–112, 1997.
- [41] Owen Lockwood. An empirical review of optimization techniques for quantum variational circuits, 2022.
- [42] Pauli Virtanen, Ralf Gommers, Travis E. Oliphant, Matt Haberland, Tyler Reddy, David Cournapeau, Evgeni Burovski, Pearu Peterson, Warren Weckesser, Jonathan Bright, Stéfan J. van der Walt, Matthew Brett, Joshua Wilson, K. Jarrod Millman, Nikolay Mayorov, Andrew R. J. Nelson, Eric Jones, Robert Kern, Eric Larson, C J Carey, İlhan Polat, Yu Feng, Eric W. Moore, Jake VanderPlas, Denis Laxalde, Josef Perktold, Robert Cimrman, Ian Henriksen, E. A. Quintero, Charles R. Harris, Anne M. Archibald, Antônio H. Ribeiro, Fabian Pedregosa, Paul van Mulbregt, Aditya Vijaykumar, Alessandro Pietro Bardelli, Alex Rothberg, Andreas Hilboll, Andreas Kloeckner, Anthony Scopatz, Antony Lee, Ariel Rokem, C. Nathan Woods, Chad Fulton, Charles Masson, Christian Häggström, Clark Fitzgerald, David A. Nicholson, David R. Hagen, Dmitrii V. Pasechnik, Emanuele Olivetti, Eric Martin, Eric Wieser, Fabrice Silva, Felix Lenders, Florian Wilhelm, G. Young, Gavin A. Price, Gert-Ludwig Ingold, Gregory E. Allen, Gregory R. Lee, Hervé Audren, Irvin Probst, Jörg P. Dietrich, Jacob Silterra, James T Webber, Janko Slavič, Joel Nothman, Johannes Buchner, Johannes Kulick, Johannes L. Schönberger, José Vinícius de Miranda Cardoso, Joscha Reimer, Joseph Harrington, Juan Luis Cano Rodríguez, Juan Nunez-Iglesias, Justin Kuczynski, Kevin Tritz, Martin Thoma, Matthew Newville, Matthias Kümmerer, Maximilian Bolingbroke, Michael Tartre, Mikhail Pak, Nathaniel J. Smith, Nikolai Nowaczyk, Nikolay Shebanov, Oleksandr Pavlyk, Per A. Brodtkorb, Perry Lee, Robert T. McGibbon, Roman Feldbauer, Sam Lewis, Sam Tygier, Scott Sievert, Sebastiano Vigna, Stefan Peterson, Surhud More, Tadeusz Pudlik, Takuya Oshima, Thomas J. Pingel, Thomas P. Robitaille, Thomas Spura, Thouis R. Jones, Tim Cera, Tim Leslie, Tiziano Zito, Tom Krauss, Utkarsh Upadhyay, Yaroslav O. Halchenko, and Yoshiki Vázquez-Baeza. Scipy 1.0: fundamental algorithms for scientific computing in python. *Nature Methods*, 17(3):261–272, 2020.
- [43] Wim Lavrijsen, Ana Tudor, Juliane Muller, Costin Iancu, and Wibe de Jong. Classical optimizers for noisy intermediate-scale quantum devices, 2020.
- [44] Kevin J Sung, Jiahao Yao, Matthew P Harrigan, Nicholas C Rubin, Zhang Jiang, Lin Lin, Ryan Babbush, and Jarrod R McClean. Using models to improve optimizers for variational quantum algorithms. *Quantum Science and Technology*, 5(4):044008, 2020.
- [45] Ryan Shaffer, Lucas Kocia, and Mohan Sarovar. Surrogate-based optimization for variational quantum algorithms. *Physical Review A*, 107(3), March 2023.

- [46] Zhaoqi Leng, Pranav Mundada, Saeed Ghadimi, and Andrew Houck. Robust and efficient algorithms for high-dimensional black-box quantum optimization, 2019.
- [47] Jiahao Yao, Marin Bukov, and Lin Lin. Policy gradient based quantum approximate optimization algorithm, 2020.
- [48] Giacomo Nannicini. Performance of hybrid quantum-classical variational heuristics for combinatorial optimization. *Physical Review E*, 99(1), January 2019.
- [49] Jonathan Romero, Ryan Babbush, Jarrod R. McClean, Cornelius Hempel, Peter Love, and Alán Aspuru-Guzik. Strategies for quantum computing molecular energies using the unitary coupled cluster ansatz, 2018.
- [50] John A. Nelder and Roger Mead. A simplex method for function minimization. *Comput. J.*, 7:308–313, 1965.
- [51] J.C. Spall. Multivariate stochastic approximation using a simultaneous perturbation gradient approximation. *IEEE Transactions on Automatic Control*, 37(3):332–341, 1992.
- [52] Jorge Nocedal and Stephen J. Wright. *Numerical Optimization*. Springer, New York, NY, USA, 2e edition, 2006.
- [53] John Duchi, Elad Hazan, and Yoram Singer. Adaptive subgradient methods for online learning and stochastic optimization. *Journal of Machine Learning Research*, 12(61):2121–2159, 2011.
- [54] Alex Graves. Generating sequences with recurrent neural networks, 2014.
- [55] H. McMahan, Gary Holt, Michael Young, Dietmar Ebner, Julian Grady, Lan Nie, Todd Phillips, Eugene Davydov, Daniel Golovin, Sharat Chikkerur, Dan Liu, Martin Wattenberg, Arnar Hrafnkelsson, Tom Boulos, and Jeremy Kubica. Ad click prediction: a view from the trenches, 08 2013.
- [56] Sashank J. Reddi, Satyen Kale, and Sanjiv Kumar. On the convergence of adam and beyond, 2019.
- [57] Timothy Dozat. Incorporating nesterov momentum into adam, 2016.
- [58] Diederik P. Kingma and Jimmy Ba. Adam: A method for stochastic optimization, 2017.
- [59] Roger Fletcher and M. J. D. Powell. A rapidly convergent descent method for minimization. *Comput. J.*, 6:163–168, 1963.
- [60] David F. Shanno. Conditioning of quasi-newton methods for function minimization. *Mathematics of Computation*, 24:647–656, 1970.
- [61] Andrew R. Conn, Nicholas I. M. Gould, and Philippe L. Toint. Convergence of quasi-newton matrices generated by the symmetric rank one update. *Mathematical Programming*, 50:177–195, 1991.
- [62] Hanif D Sherali and Osman Ulular. Conjugate gradient methods using quasi-newton updates with inexact line searches. *Journal of Mathematical Analysis and Applications*, 150(2):359–377, 1990.
- [63] Brian Irwin and Eldad Haber. Secant penalized bfgs: a noise robust quasi-newton method via penalizing the secant condition. *Computational Optimization and Applications*, 84(3):651–702, 2023.
- [64] Shun ichi Amari. Backpropagation and stochastic gradient descent method. *Neurocomputing*, 5(4):185–196, 1993.
- [65] Shun-ichi Amari. Natural Gradient Works Efficiently in Learning. *Neural Computation*, 10(2):251–276, 02 1998.
- [66] James Stokes, Josh Izaac, Nathan Killoran, and Giuseppe Carleo. Quantum natural gradient. *Quantum*, 4:269, 2020.
- [67] Julien Gacon, Christa Zoufal, Giuseppe Carleo, and Stefan Woerner. Simultaneous perturbation stochastic approximation of the quantum fisher information. *Quantum*, 5:567, 2021.
- [68] David Fitzek, Robert S. Jonsson, Werner Dobrautz, and Christian Schäfer. Optimizing variational quantum algorithms with qbang: Efficiently interweaving metric and momentum to navigate flat energy landscapes. *Quantum*, 8:1313, 2024.
- [69] Francisco Escudero, David Fernández-Fernández, Gabriel Jaumà, Guillermo F. Peñas, and Luciano Pereira. Hardware-efficient entangled measurements for variational quantum algorithms. *Physical Review Applied*, 20(3), September 2023.
- [70] Abhinav Kandala, Antonio Mezzacapo, Kristan Temme, Maika Takita, Markus Brink, Jerry M. Chow, and Jay M. Gambetta. Hardware-efficient variational quantum eigensolver for small molecules and quantum magnets. *Nature*, 549(7671):242–246, September 2017.
- [71] Pablo Díez-Valle, Diego Porras, and Juan José García-Ripoll. Quantum variational optimization: The role of entanglement and problem hardness. *Physical Review A*, 104(6), December 2021.
- [72] Ion Necoara, Y. Nesterov y, and François Glineur. A random coordinate descent method on large-scale optimization problems with linear constraints, 2013.
- [73] Zhiyan Ding, Taehee Ko, Jiahao Yao, Lin Lin, and Xiantao Li. Random coordinate descent: a simple alternative for optimizing parameterized quantum circuits, 2023.
- [74] YoungJun Yoo. Hyperparameter optimization of deep neural network using univariate dynamic encoding algorithm for searches. *Knowledge-Based Systems*, 178:74–83, 2019.
- [75] Lisha Li, Kevin Jamieson, Giulia DeSalvo, Afshin Rostamizadeh, and Ameet Talwalkar. Hyperband:

- A novel bandit-based approach to hyperparameter optimization, 2018.
- [76] Petro Liashchynskiy and Pavlo Liashchynskiy. Grid search, random search, genetic algorithm: A big comparison for nas, 2019.
  - [77] Matthias Feurer, Aaron Klein, Katharina Eggensperger, Jost Springenberg, Manuel Blum, and Frank Hutter. Efficient and robust automated machine learning. In C. Cortes, N. Lawrence, D. Lee, M. Sugiyama, and R. Garnett, editors, *Advances in Neural Information Processing Systems*, volume 28. Curran Associates, Inc., 2015.
  - [78] Jasper Snoek, Hugo Larochelle, and Ryan P. Adams. Practical bayesian optimization of machine learning algorithms, 2012.
  - [79] Bobak Shahriari, Kevin Swersky, Ziyu Wang, Ryan P. Adams, and Nando de Freitas. Taking the human out of the loop: A review of bayesian optimization. *Proceedings of the IEEE*, 104(1):148–175, 2016.
  - [80] R. W. Hamming. Error detecting and error correcting codes. *Bell System Technical Journal*, 29(2):147–160, 1950.
  - [81] Aram W. Harrow, Avinatan Hassidim, and Seth Lloyd. Quantum algorithm for linear systems of equations. *Physical Review Letters*, 103(15), 2009.
  - [82] C.L. Degen, F. Reinhard, and P. Cappellaro. Quantum sensing. *Reviews of Modern Physics*, 89(3), 2017.
  - [83] Philippe Faist, Mischa P. Woods, Victor V. Albert, Joseph M. Renes, Jens Eisert, and John Preskill. Time-energy uncertainty relation for noisy quantum metrology. *PRX Quantum*, 4(4), 2023.
  - [84] Yunfei Wang and Junyu Liu. A comprehensive review of quantum machine learning: from nisq to fault tolerance, 2024.
  - [85] Mateusz Ostaszewski, Edward Grant, and Marcello Benedetti. Structure optimization for parameterized quantum circuits. *Quantum*, 5:391, 2021.
  - [86] Sara Fridovich-Keil and Benjamin Recht. Approximately exact line search, 2022.
  - [87] Hardik Tankaria, Shinji Sugimoto, and Nobuo Yamashita. A regularized limited memory bfgs method for large-scale unconstrained optimization and its efficient implementations, 2021.
  - [88] Hong Hui Tan and King Hann Lim. Review of second-order optimization techniques in artificial neural networks backpropagation. *IOP Conference Series: Materials Science and Engineering*, 495(1):012003, apr 2019.
  - [89] Maria Schuld, Ville Bergholm, Christian Gogolin, Josh Izaac, and Nathan Killoran. Evaluating analytic gradients on quantum hardware. *Phys. Rev. A*, 99:032331, Mar 2019.
  - [90] Andrea Mari, Thomas R. Bromley, and Nathan Killoran. Estimating the gradient and higher-order derivatives on quantum hardware. *Physical Review A*, 103(1), January 2021.
  - [91] David Wierichs, Josh Izaac, Cody Wang, and Cedric Yen-Yu Lin. General parameter-shift rules for quantum gradients. *Quantum*, 6:677, 2022.
  - [92] J. E. Dennis, Jr. and Jorge J. Moré. Quasi-newton methods, motivation and theory. *SIAM Review*, 19(1):46–89, 1977.
  - [93] Albert S. Berahas and Martin Takáč. A robust multi-batch l-bfgs method for machine learning, 2019.
  - [94] Jascha Sohl-Dickstein, Ben Poole, and Surya Ganguli. Fast large-scale optimization by unifying stochastic gradient and quasi-newton methods, 2014.
  - [95] Hanif D Sherali and Osman Ulular. Conjugate gradient methods using quasi-newton updates with inexact line searches. *Journal of Mathematical Analysis and Applications*, 150(2):359–377, 1990.
  - [96] C. G. Broyden. A class of methods for solving nonlinear simultaneous equations. *Mathematics of Computation*, 19:577–593, 1965.
  - [97] Robert M. Freund. Penalty and barrier methods for constrained optimization, 2004.
  - [98] J Lambert and E S Sørensen. From classical to quantum information geometry: a guide for physicists. *New Journal of Physics*, 25(8):081201, 2023.
  - [99] Johannes Jakob Meyer. Fisher information in noisy intermediate-scale quantum applications. *Quantum*, 5:539, September 2021.
  - [100] David Wierichs, Christian Gogolin, and Michael Kastoryano. Avoiding local minima in variational quantum eigensolvers with the natural gradient optimizer. *Physical Review Research*, 2(4), 2020.
  - [101] Jacob L. Beckey, M. Cerezo, Akira Sone, and Patrick J. Coles. Variational quantum algorithm for estimating the quantum fisher information. *Physical Review Research*, 4(1), February 2022.
  - [102] Julien Gacon, Jannes Nys, Riccardo Rossi, Stefan Woerner, and Giuseppe Carleo. Variational quantum time evolution without the quantum geometric tensor. *Physical Review Research*, 6(1), February 2024.
  - [103] David Fitzek, Robert S. Jonsson, Werner Dobrautz, and Christian Schäfer. Optimizing Variational Quantum Algorithms with qBang: Efficiently Interweaving Metric and Momentum to Navigate Flat Energy Landscapes. *Quantum*, 8:1313, 2024.
  - [104] Boris Polyak. Some methods of speeding up the convergence of iteration methods. *Ussr Computational Mathematics and Mathematical Physics*, 4:1–17, 1964.

- [105] Ilya Sutskever, James Martens, George Dahl, and Geoffrey Hinton. On the importance of initialization and momentum in deep learning. In *Proceedings of the 30th International Conference on International Conference on Machine Learning - Volume 28*, ICML'13, page III–1139–III–1147. JMLR.org, 2013.
- [106] Wei Tao, Sheng Long, Gaowei Wu, and Qing Tao. The role of momentum parameters in the optimal convergence of adaptive polyak’s heavy-ball methods, 2021.
- [107] Goran Nakerst, John Brennan, and Masudul Haque. Gradient descent with momentum — to accelerate or to super-accelerate?, 2020.
- [108] H Park, S.-I Amari, and K Fukumizu. Adaptive natural gradient learning algorithms for various stochastic models. *Neural Networks*, 13(7):755–764, 2000.
- [109] Sidhartha Dash, Filippo Vicentini, Michel Ferrero, and Antoine Georges. Efficiency of neural quantum states in light of the quantum geometric tensor, 2024.
- [110] Diederik P. Kingma and Jimmy Ba. Adam: A method for stochastic optimization, 2017.
- [111] Tong Yu and Hong Zhu. Hyper-parameter optimization: A review of algorithms and applications, 2020.
- [112] Bernd Bischl, Martin Binder, Michel Lang, Tobias Pielok, Jakob Richter, Stefan Coors, Janek Thomas, Theresa Ullmann, Marc Becker, Anne-Laure Boulesteix, Difan Deng, and Marius Lindauer. Hyperparameter optimization: Foundations, algorithms, best practices and open challenges, 2021.
- [113] Emilio Porcu, Moreno Bevilacqua, Robert Schaback, and Chris J. Oates. The matérn model: A journey through statistics, numerical analysis and machine learning, 2023.
- [114] H. J. Kushner. A New Method of Locating the Maximum Point of an Arbitrary Multipeak Curve in the Presence of Noise. *Journal of Basic Engineering*, 86(1):97–106, 03 1964.
- [115] T.L Lai and Herbert Robbins. Asymptotically efficient adaptive allocation rules. *Advances in Applied Mathematics*, 6(1):4–22, 1985.
- [116] Peter Auer. Using confidence bounds for exploitation-exploration trade-offs, mar 2003.
- [117] Eric Brochu, Matthew W. Hoffman, and Nando de Freitas. Portfolio allocation for bayesian optimization, 2011.
- [118] Thiago de P. Vasconcelos, Daniel Augusto R.M.A. de Souza, Gustavo C. de M. Virgolino, César L.C. Mattos, and João P.P. Gomes. Self-tuning portfolio-based bayesian optimization. *Expert Systems with Applications*, 188:115847, 2022.
- [119] The dimacs optimization implementation challenge. <http://dimacs.rutgers.edu/programs/challenge/>. Accessed: 2024-06-21.
- [120] Le challenge roaDef, archives. <https://www.roaDef.org/challenge/2022/en/index.php>. Accessed: 2024-06-21.
- [121] Mahyar Fazlyab, Alexander Robey, Hamed Hassani, Manfred Morari, and George J. Pappas. Efficient and accurate estimation of lipschitz constants for deep neural networks, 2023.
- [122] Yuezhu Xu and S. Sivaranjani. Compositional estimation of lipschitz constants for deep neural networks, 2024.
- [123] Calypso Herrera, Florian Krach, and Josef Teichmann. Local lipschitz bounds of deep neural networks, 2023.
- [124] C. Walck. *Hand-book on Statistical Distributions for Experimentalists*. Stockholms universitet, 1996.
- [125] C. O. S. Sorzano, J. Vargas, and A. Pascual Montano. A survey of dimensionality reduction techniques, 2014.
- [126] Ella Bingham and Heikki Mannila. Random projection in dimensionality reduction: applications to image and text data. In *Proceedings of the Seventh ACM SIGKDD International Conference on Knowledge Discovery and Data Mining*, KDD '01, page 245–250, New York, NY, USA, 2001. Association for Computing Machinery.

## A Algorithmic complement

---

**Algorithm 2** SP-BFGS implementation, integration with the Amijo-Wolf backtracking implementation. *compute\_linear* function is the expression in adapting  $\beta_i$  as a function of the measured gradient at iteration  $i$ , for example with interception or noise model in 16

---

```

1: Input:  $f, \beta\_compute\_linear, x_{init}, \alpha, \beta_{reduce}, c_0, c_1, N_0, N_s, MAXIT$ 
2: Output:  $x, best\_value$ 
3:  $x \leftarrow x_{init}$ 
4:  $i \leftarrow 0$ 
5:  $H_i \leftarrow$  Identity Matrix
6: while  $i < MAXIT$  do
7:    $\nabla_i \leftarrow \nabla_\theta f(x)$ 
8:   if  $\|\nabla_i\| < tol$  then
9:     break
10:  end if
11:   $p_i \leftarrow -H_i \cdot \nabla_i$ 
12:  while not satisfying Armijo-Wolfe condition do
13:    if  $f(x + \alpha p_i) \leq f(x) + c_0 \alpha \cdot \nabla_i^T p_i$  then
14:      break
15:    end if
16:    if  $-p_i^T \nabla_\theta f(x + \alpha p_i) \leq -c_1 p_i^T \nabla_i$  then
17:      break
18:    end if
19:     $\alpha \leftarrow \beta_{reduce} \cdot \alpha$ 
20:  end while
21:   $x_i \leftarrow x + \alpha p_i$ 
22:   $s_i \leftarrow x_i - x$ 
23:   $\nabla_{i+} \leftarrow \nabla f(x_i)$ 
24:   $y_i \leftarrow \nabla_{i+} - \nabla_i$ 
25:   $\beta_i \leftarrow \beta\_compute\_linear(N_0, N_s, s_i)$ 
26:   $proj \leftarrow s_i^T \cdot y_i$ 
27:   $\gamma_i \leftarrow \frac{1}{proj + \frac{1}{\beta_i}}, \quad \omega_i \leftarrow \frac{1}{proj + \frac{2}{\beta_i}}$ 
28:   $H_{ns} \leftarrow (I - \omega_i(s_i \odot y_i)) \cdot H_i(I - \omega_i(y_i \odot s_i))$ 
29:   $H_{nc} \leftarrow \omega_i \cdot \left( \frac{\gamma_i}{\omega_i} + (\gamma_i - \omega_i) \cdot y_i^T \cdot H_i y_i \right) \cdot s_i s_i^T$ 
30:   $H_n \leftarrow H_{ns} + H_{nc}$ 
31:   $x \leftarrow x_i$ 
32:   $H_i \leftarrow H_n$ 
33:   $i \leftarrow i + 1$ 
34: end while
35: return  $x$ 

```

---



## B Problem definition

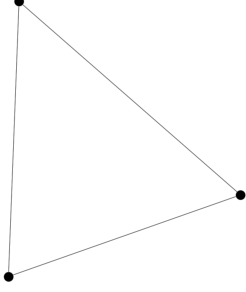


Figure 14: 3 nodes, ground solution to MaxCut: (-71.23)

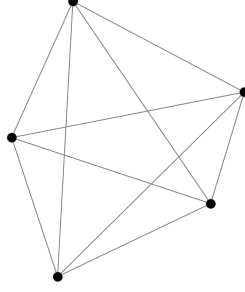


Figure 15: 5 nodes, ground solution to MaxCut: (-234.76)

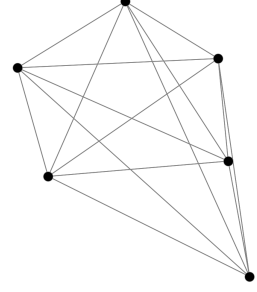


Figure 16: 6 nodes, ground solution to MaxCut: (-293.26)

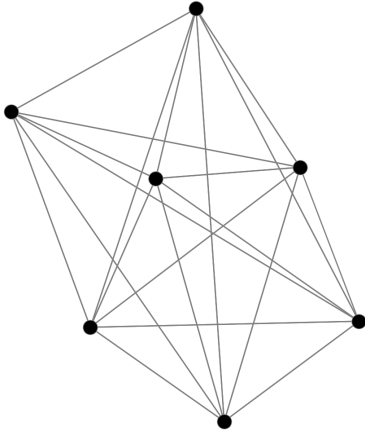


Figure 17: 7 nodes, ground solution to MaxCut: (-458.63)

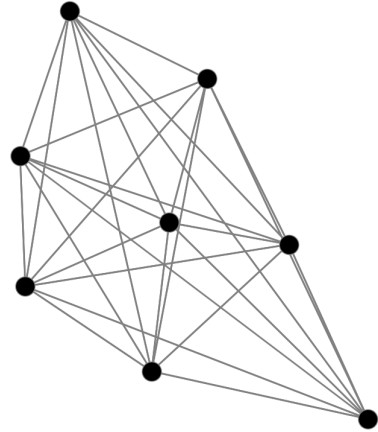


Figure 18: 8 nodes, ground solution to MaxCut: (-519.13)

Figure 19: Selected problems for benchmarking

## C Hyperparameters table

| Family              | Methods           | Params     | Search space | Defaults       |
|---------------------|-------------------|------------|--------------|----------------|
| Quasi-Newton        | BFGS              | $\alpha$   | (1e-5, 0.99) | 0.70           |
|                     |                   | $\beta$    | (0.8, 0.9)   | 0.8            |
|                     |                   | $c_1$      | (1e-5, 5)    | 0.0001         |
|                     |                   | $c_2$      | (0.1, 1)     | 1.0            |
|                     | DFP               | $\alpha$   | (1e-5, 0.99) | 0.37           |
|                     |                   | $\beta$    | (0.8, 0.9)   | 0.89           |
|                     |                   | $c_1$      | (1e-5, 5)    | 0.0017         |
|                     |                   | $c_2$      | (0.1, 1)     | 1.0            |
|                     | N-CG              | $\alpha$   | (1e-5, 0.99) | 0.99           |
|                     |                   | $\beta$    | (0.8, 0.9)   | 0.83           |
|                     |                   | $c_1$      | (1e-5, 5)    | 0.34           |
|                     |                   | $c_2$      | (0.1, 1)     | 0.59           |
|                     | SR1               | $\alpha$   | (1e-5, 0.99) | 0.48           |
|                     |                   | $\beta$    | (0.8, 0.9)   | 0.83           |
|                     |                   | $c_1$      | (1e-5, 5)    | 1e-5           |
|                     |                   | $c_2$      | (0.1, 1)     | 1.0            |
|                     | SP-BFGS           | $\alpha$   | (1e-5, 0.99) | 0.049          |
|                     |                   | $\beta$    | (0.8, 0.9)   | 0.82           |
|                     |                   | $N_0$      | (1e-5, 1)    | 1e-5           |
|                     |                   | $N_i$      | (1e-5, 1)    | 1e-5           |
|                     |                   | $c_1$      | (1e-5, 1)    | 1.67e-5        |
|                     |                   | $c_2$      | (0.1, 1)     | 1.0            |
| Quantum N. Gradient | QNG (block, diag) | $\alpha$   | (1e-5, 0.99) | 0.0016, 0.0026 |
|                     | qBroyden          | $\alpha$   | (1e-5, 0.99) | 0.0088         |
|                     |                   | $\epsilon$ | (1e-5, 0.99) | 0.0003         |
|                     | qBang             | $\alpha$   | (1e-5, 0.99) | 0.14           |
|                     |                   | $\epsilon$ | (1e-5, 0.98) | 5.06e-5        |
|                     |                   | $\beta_1$  | (1e-5, 0.99) | 0.0078         |
|                     |                   | $\beta_2$  | (1e-5, 0.99) | 0.0001         |
|                     | m-QNG             | $\alpha$   | (1e-5, 0.99) | 0.14           |
|                     |                   | $\epsilon$ | (1e-5, 0.99) | 5.06e-5        |
|                     |                   | $\beta_1$  | (1e-5, 0.99) | 0.0078         |
|                     |                   | $\beta_2$  | (1e-5, 0.99) | 0.0001         |

Table 5: Selected hyperparameters for Quasi-Newton and Quantum Natural Gradient methods.

## C.1 Full benchmark

### C.1.1 Second order quasi-Newton methods

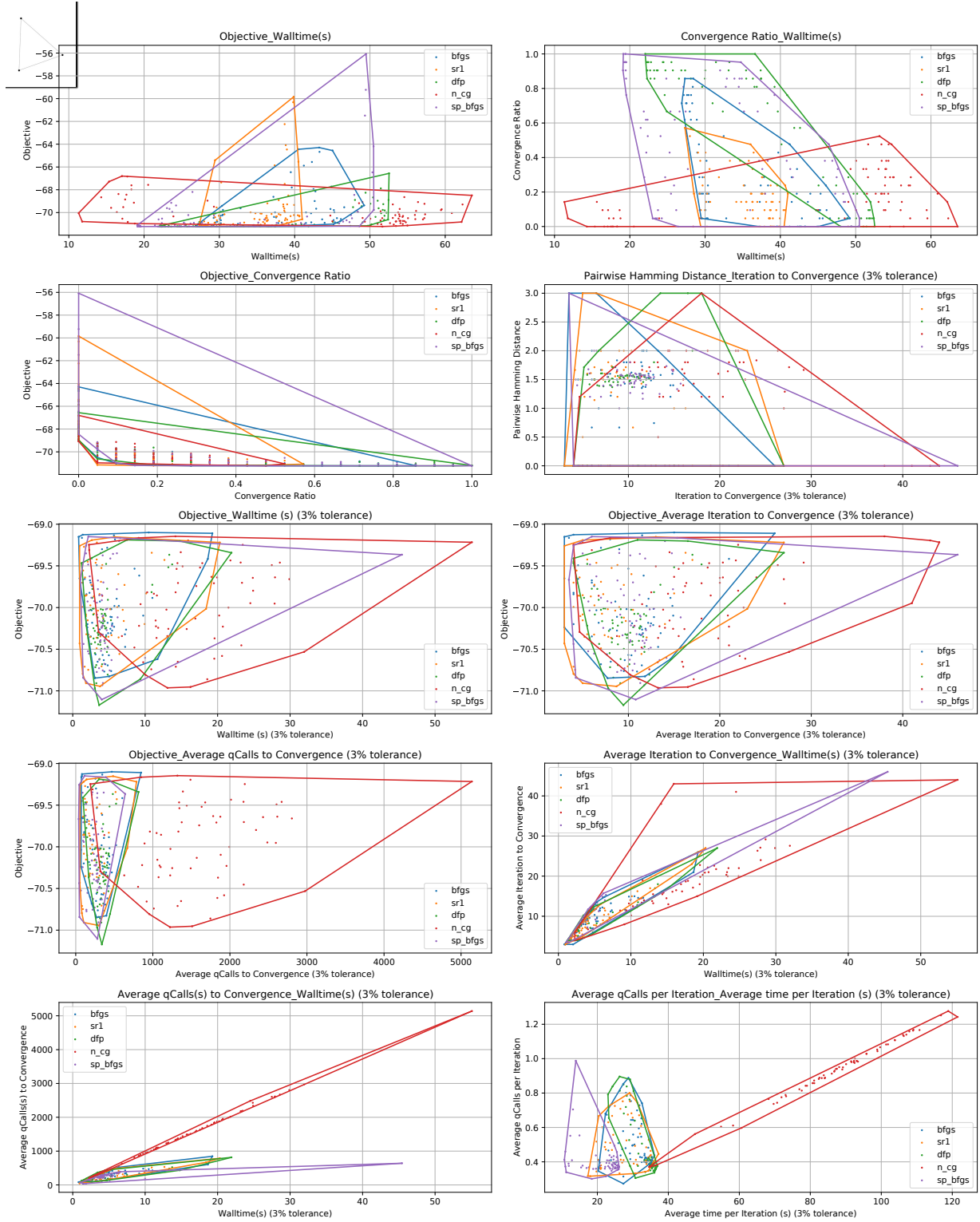


Figure 20: 3 nodes problems, 50 iterations, second order methods noiseless, 70 Bayesian sweeps

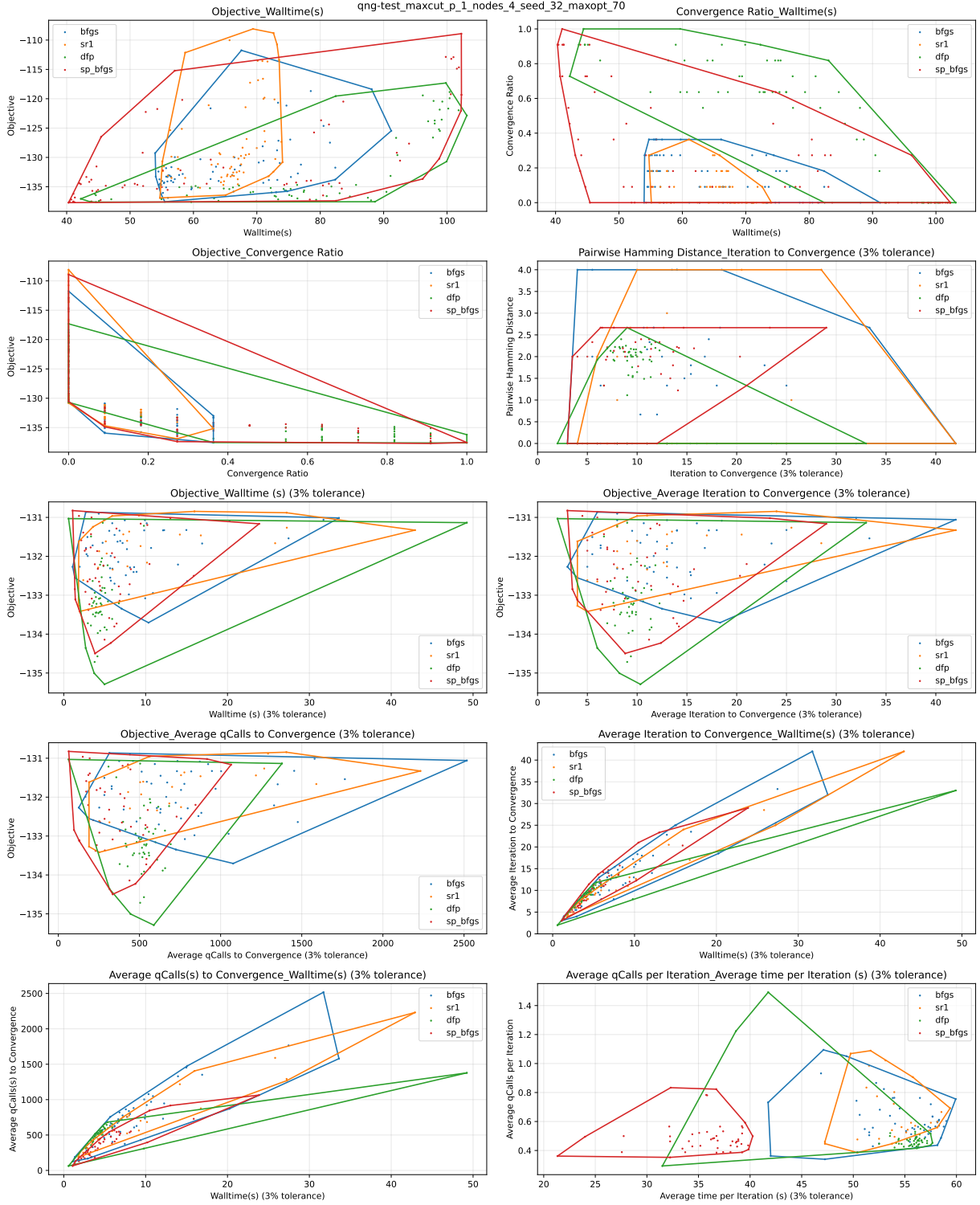


Figure 21: 4 nodes problems, 70 iterations, second order methods noiseless, 70 Bayesian sweeps

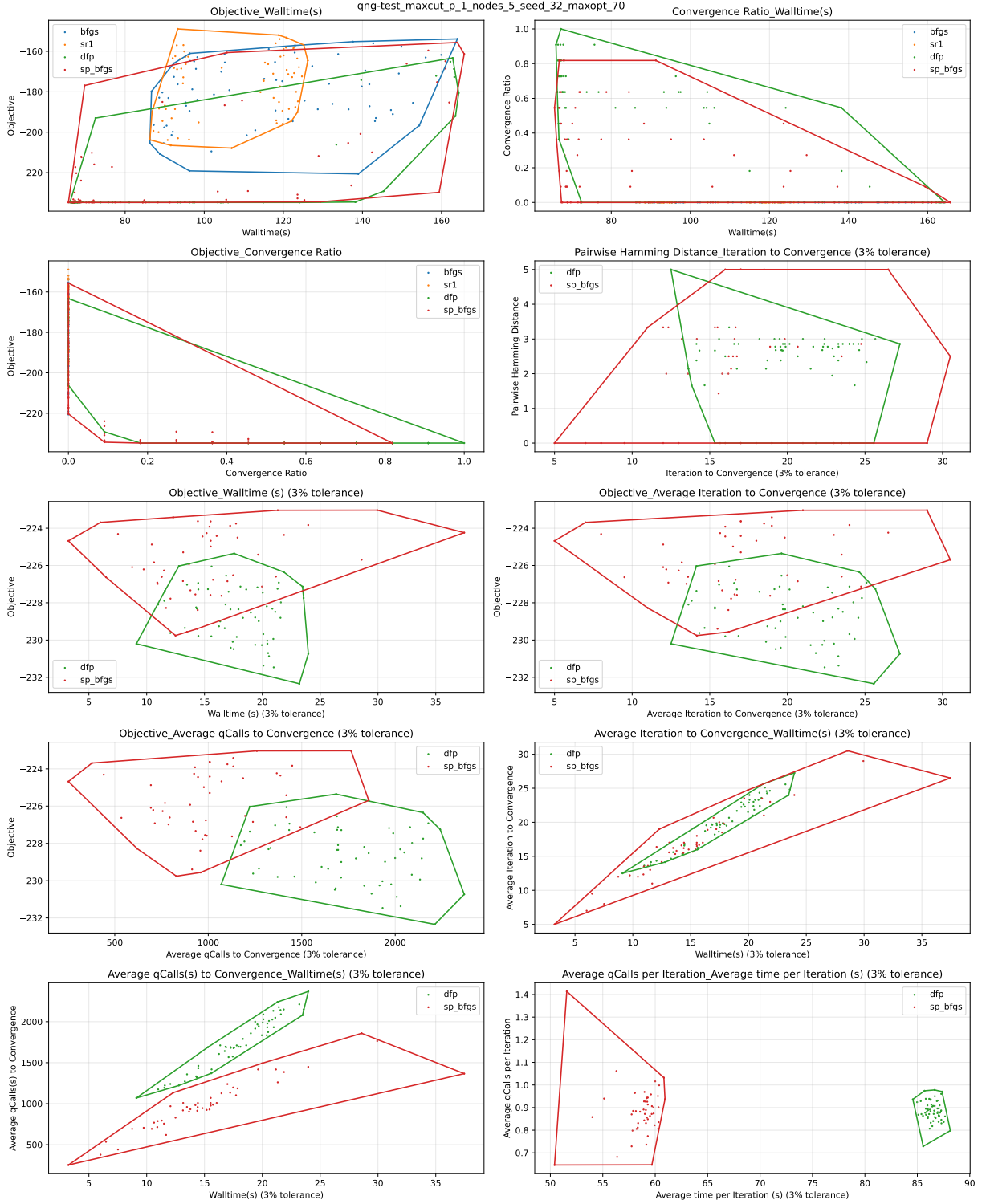


Figure 22: 5 nodes problems, 70 iterations, second order methods noiseless, 70 Bayesian sweeps

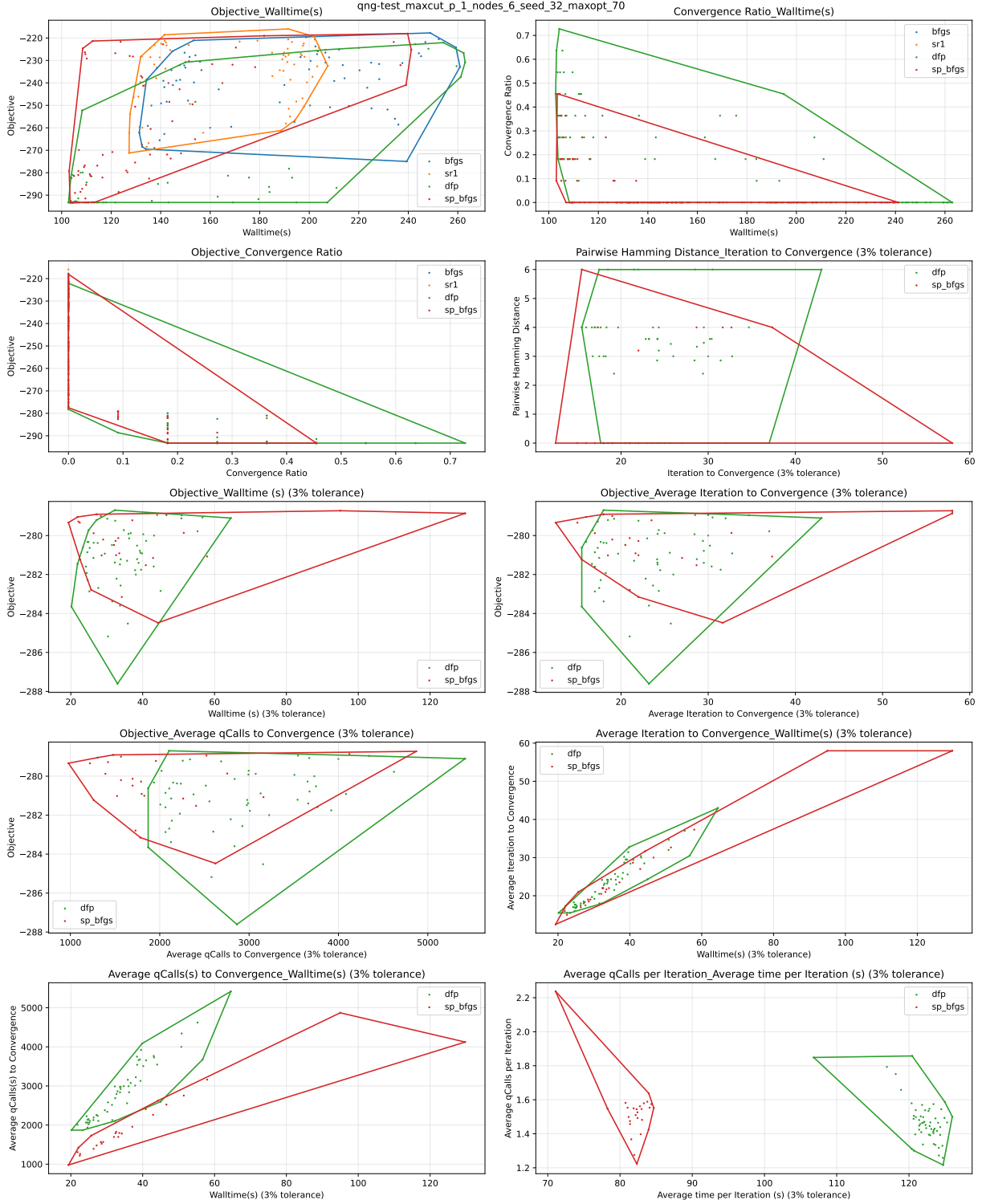


Figure 23: 6 nodes problems, 70 iterations, second order methods noiseless, 70 Bayesian sweeps

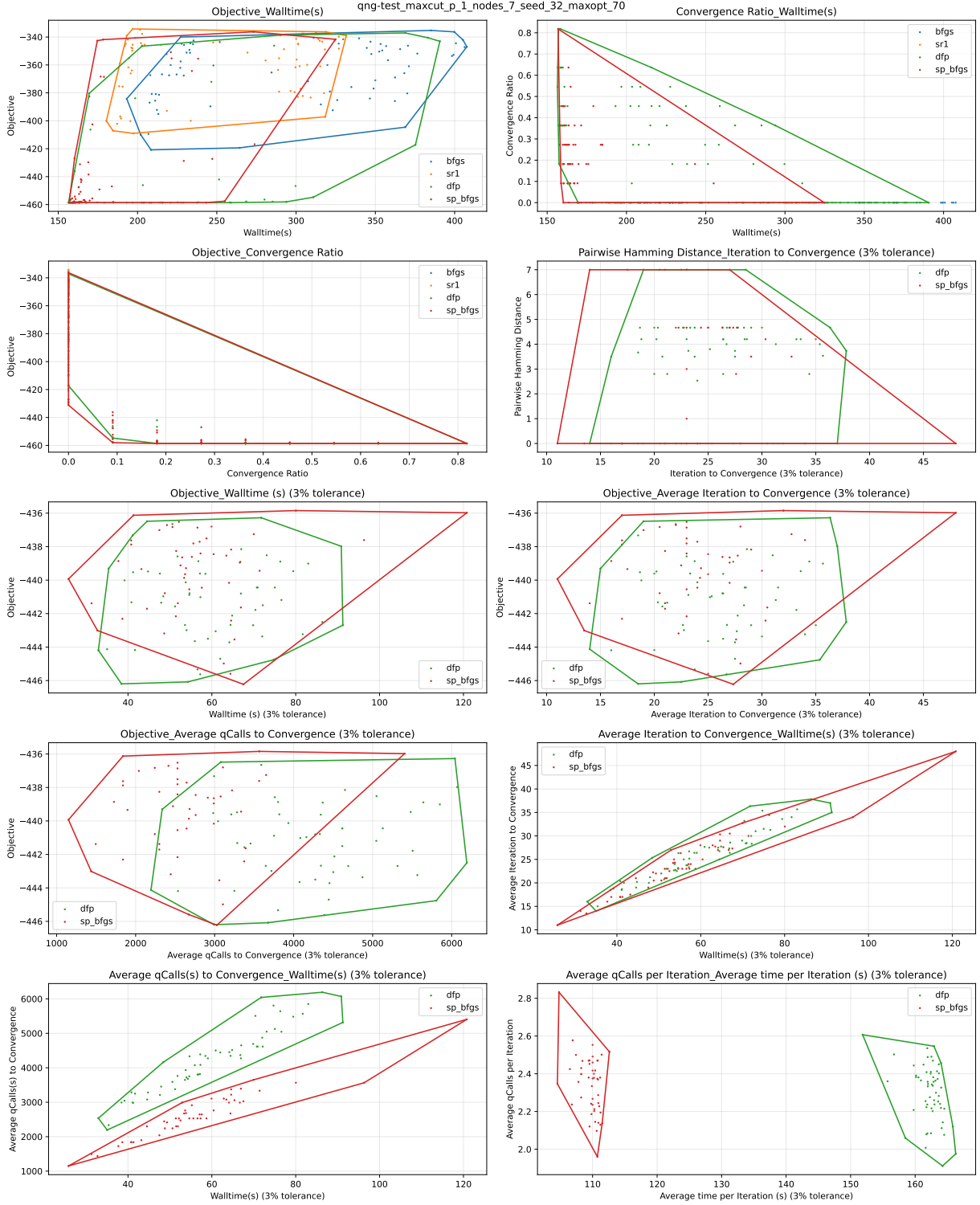


Figure 24: 7 nodes problems, 70 iterations, second order methods noiseless, 70 Bayesian sweeps

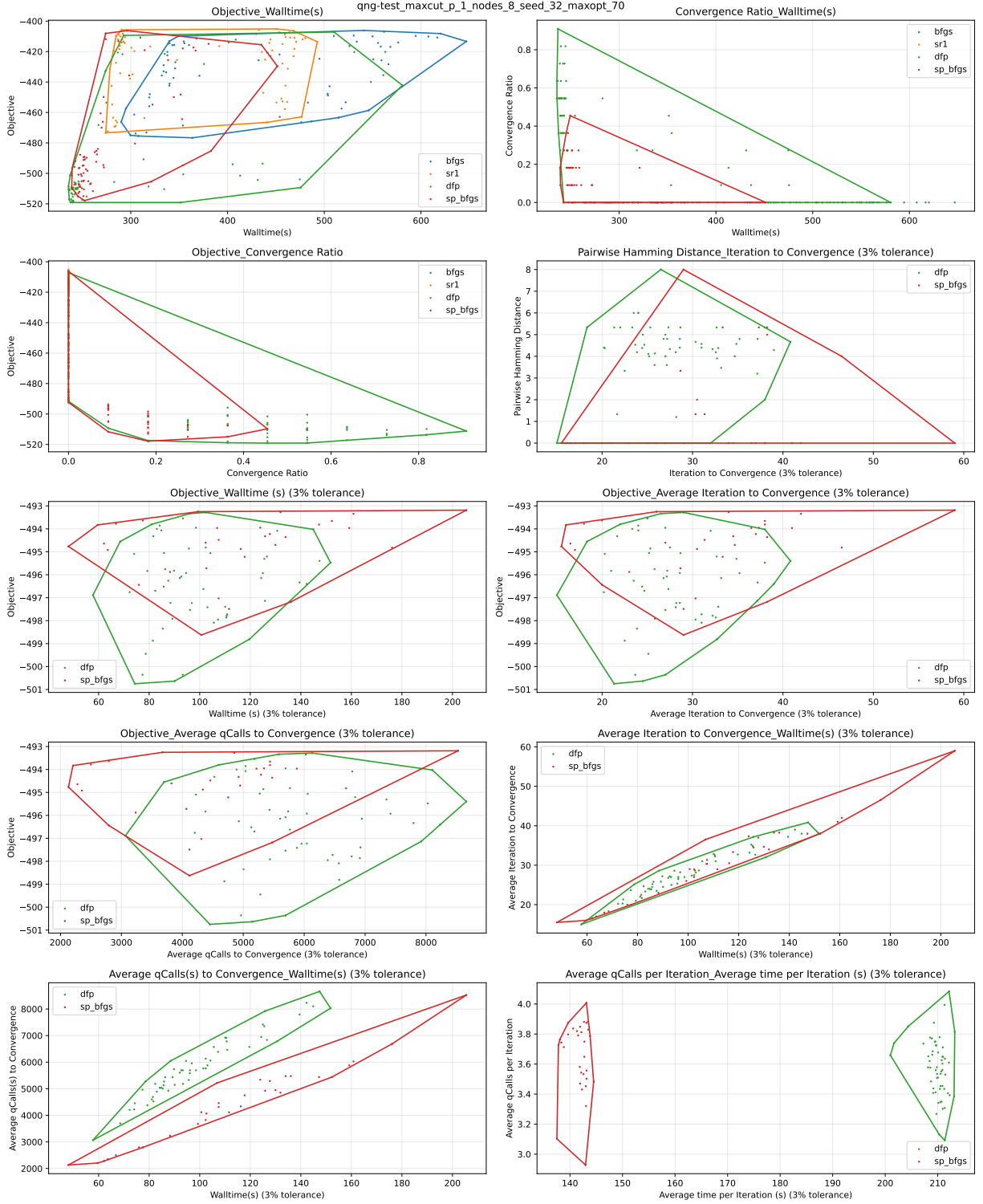


Figure 25: 8 nodes problems, 70 iterations, second order methods noiseless, 70 Bayesian sweeps



## C.1.2 Natural gradient methods

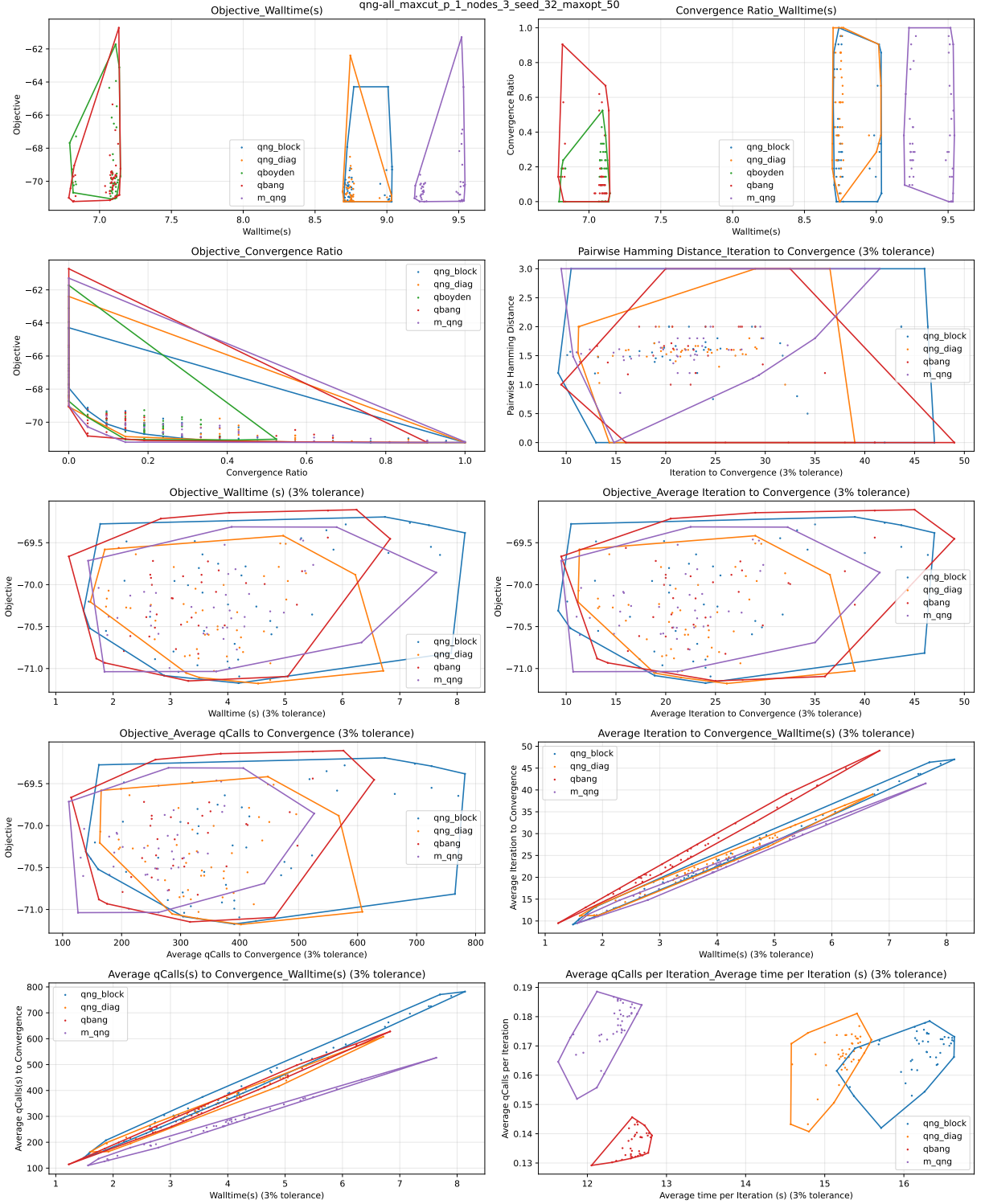


Figure 26: 3 nodes problems, 50 iterations, qng-type noiseless, 70 Bayesian runs

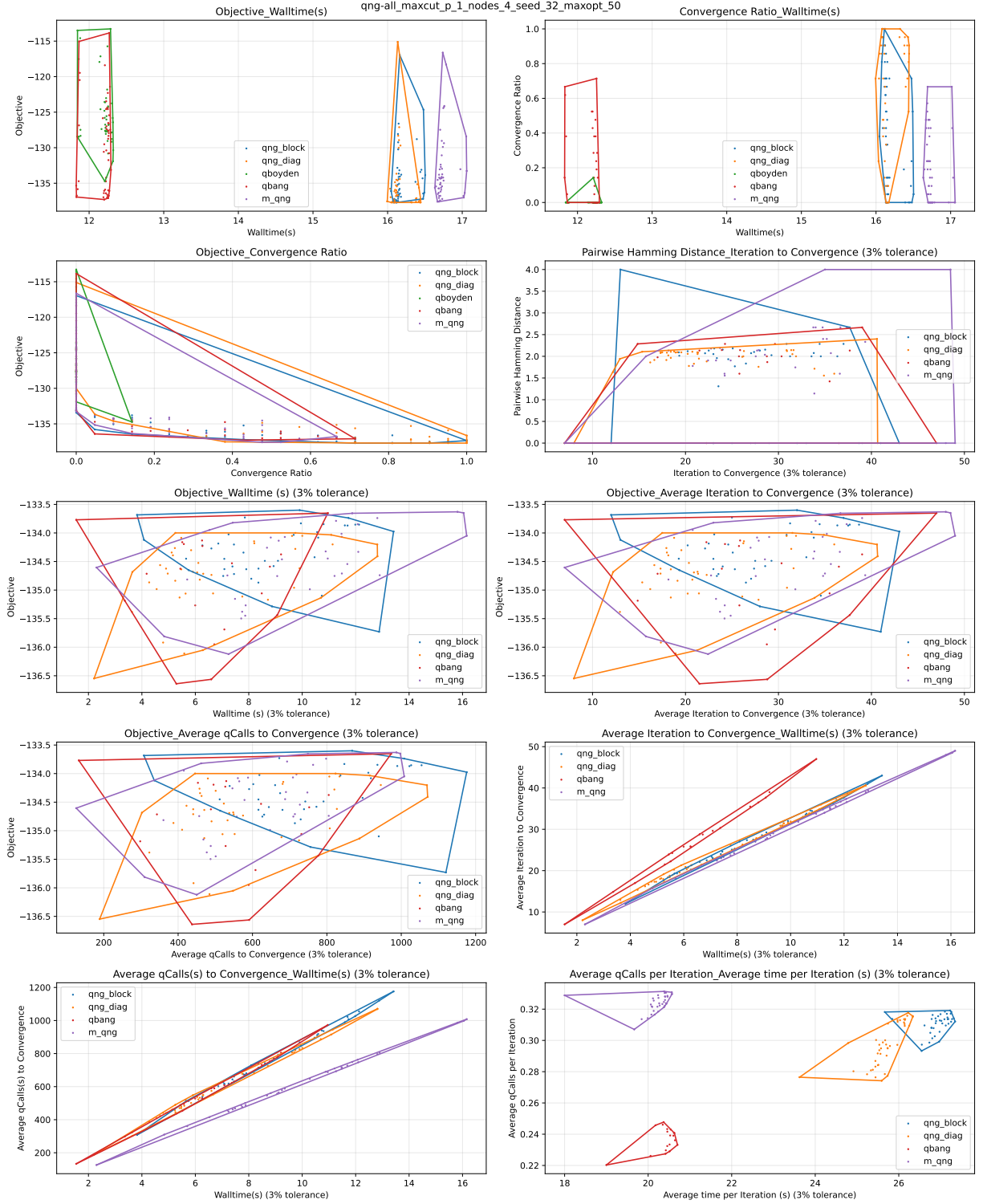


Figure 27: 4 nodes problems, 50 iterations, qng-type noiseless, 70 Bayesian runs

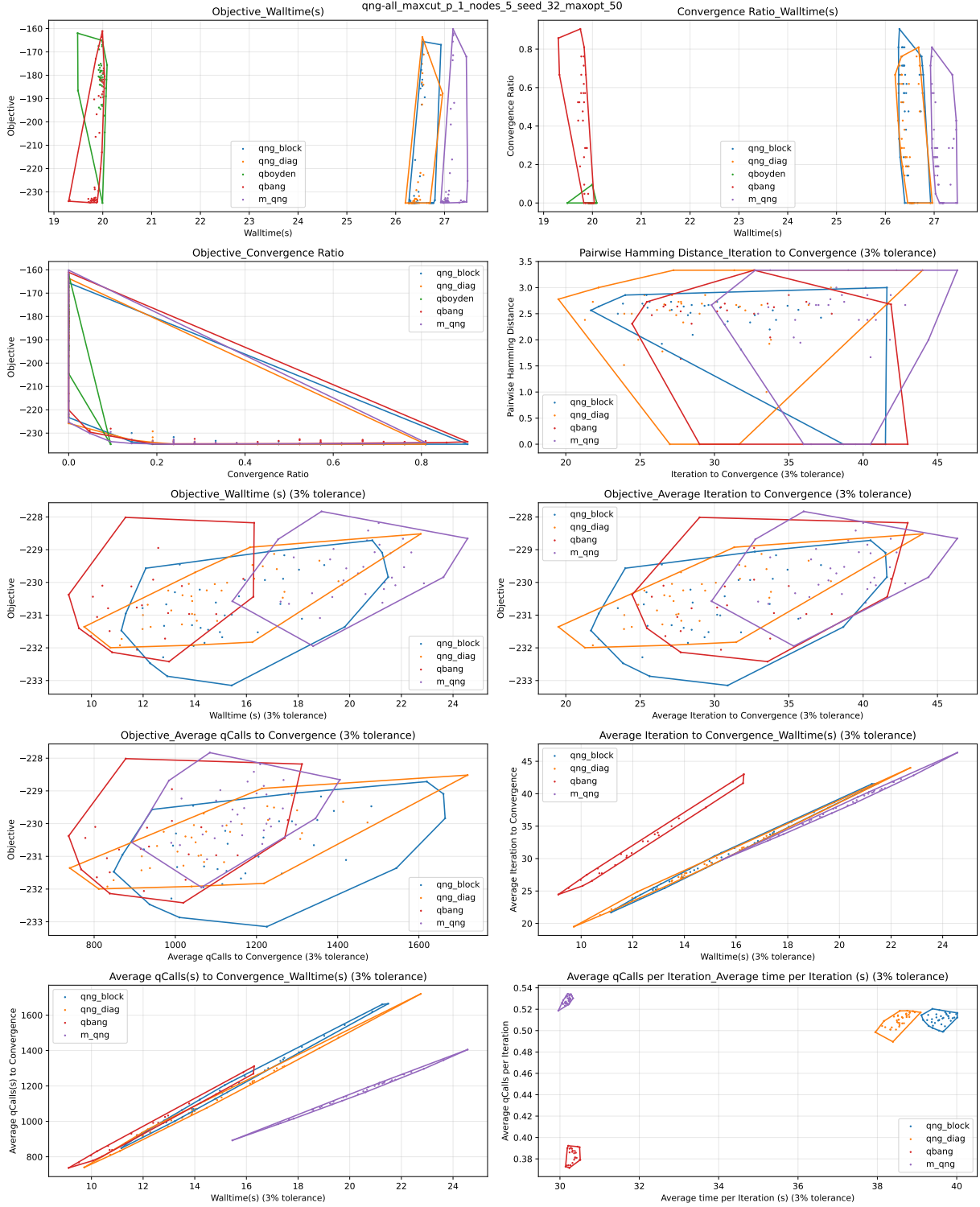


Figure 28: 5 nodes problems, 50 iterations, qng-type noiseless, 70 Bayesian runs

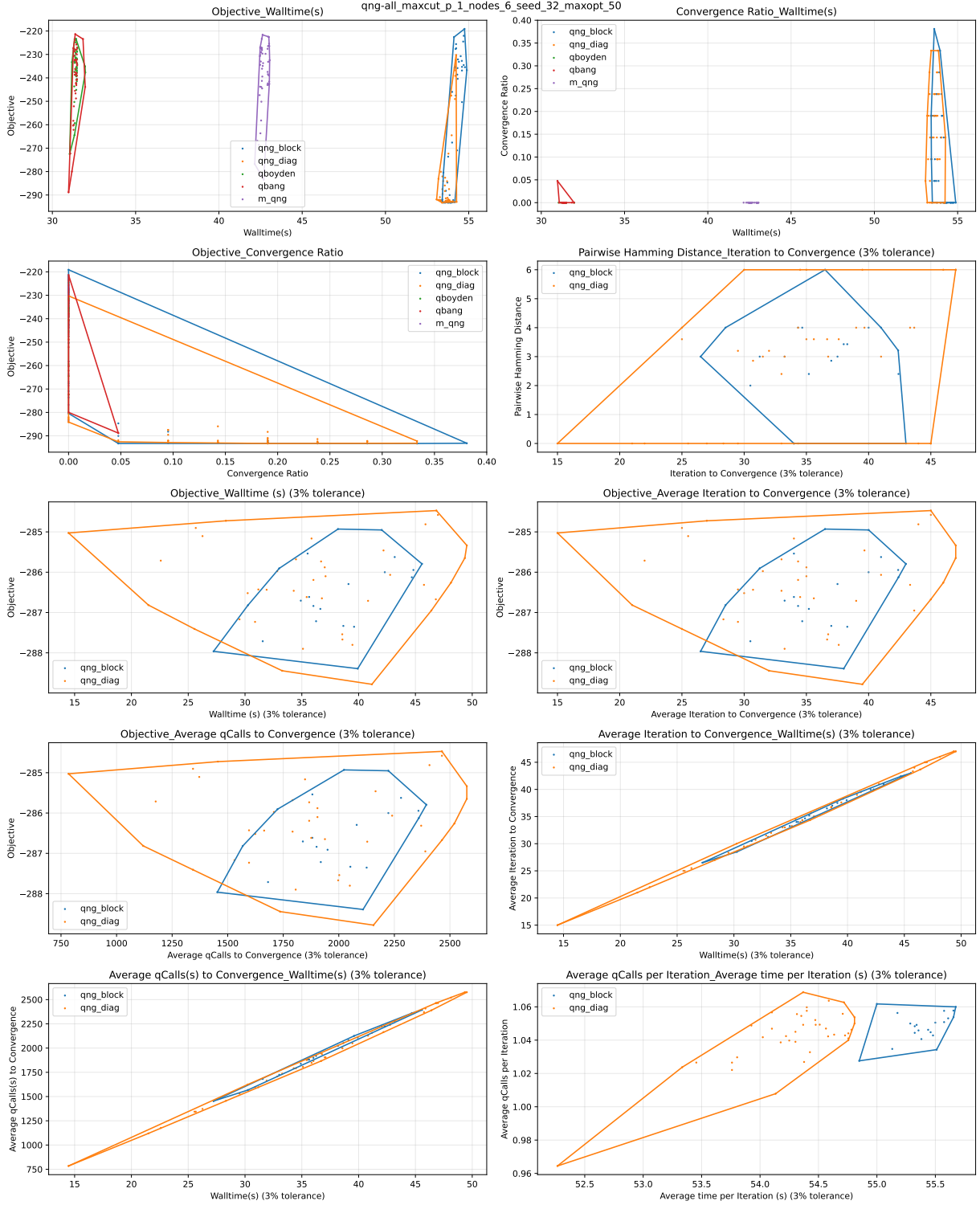


Figure 29: 6 nodes problems, 50 iterations, qng-type noiseless, 70 Bayesian runs

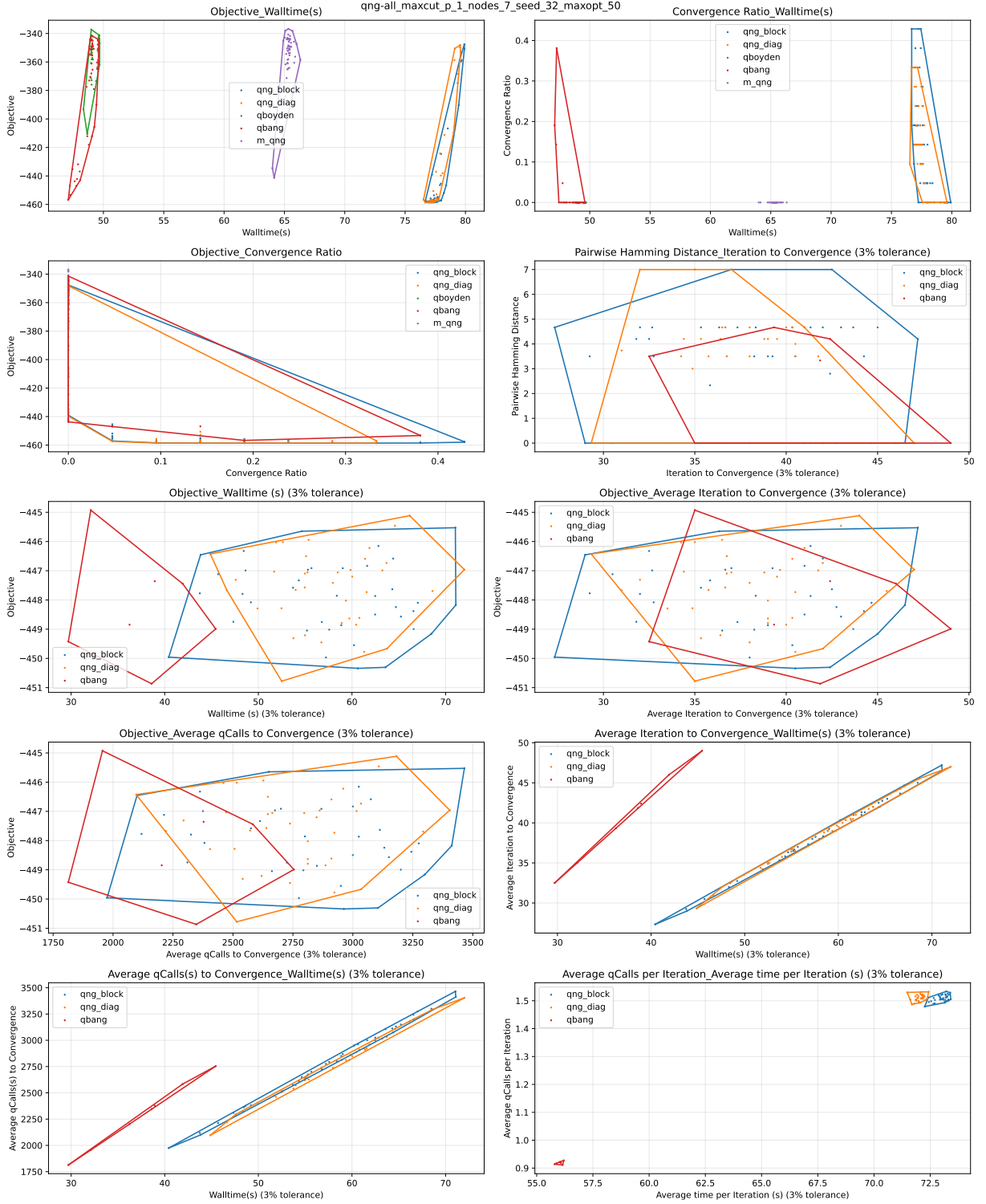


Figure 30: 7 nodes problems, 50 iterations, qng-type noiseless, 70 Bayesian runs

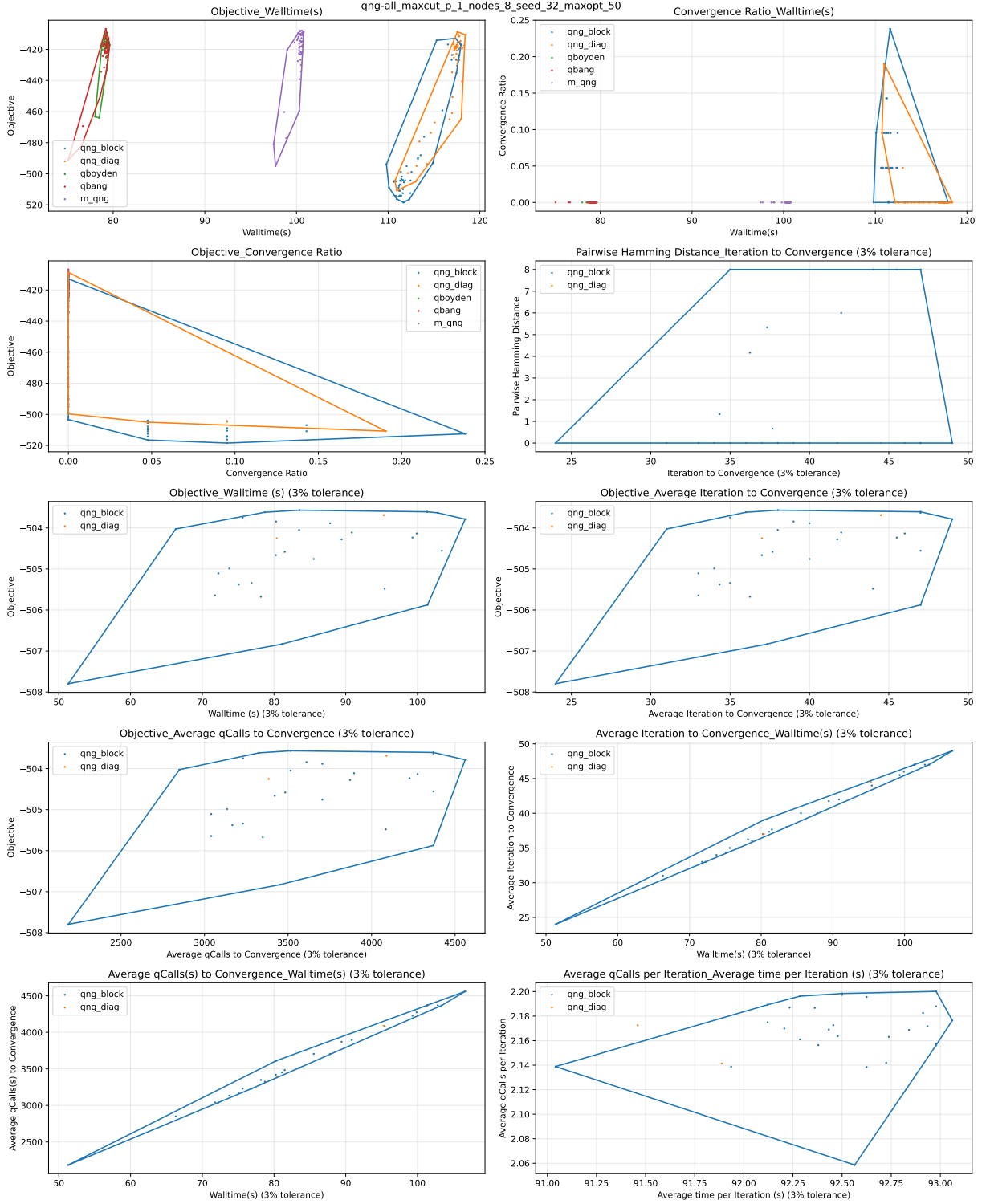


Figure 31: 8 nodes problems, 50 iterations, qng-type noiseless, 70 Bayesian runs

## C.1.3 Stochastic methods

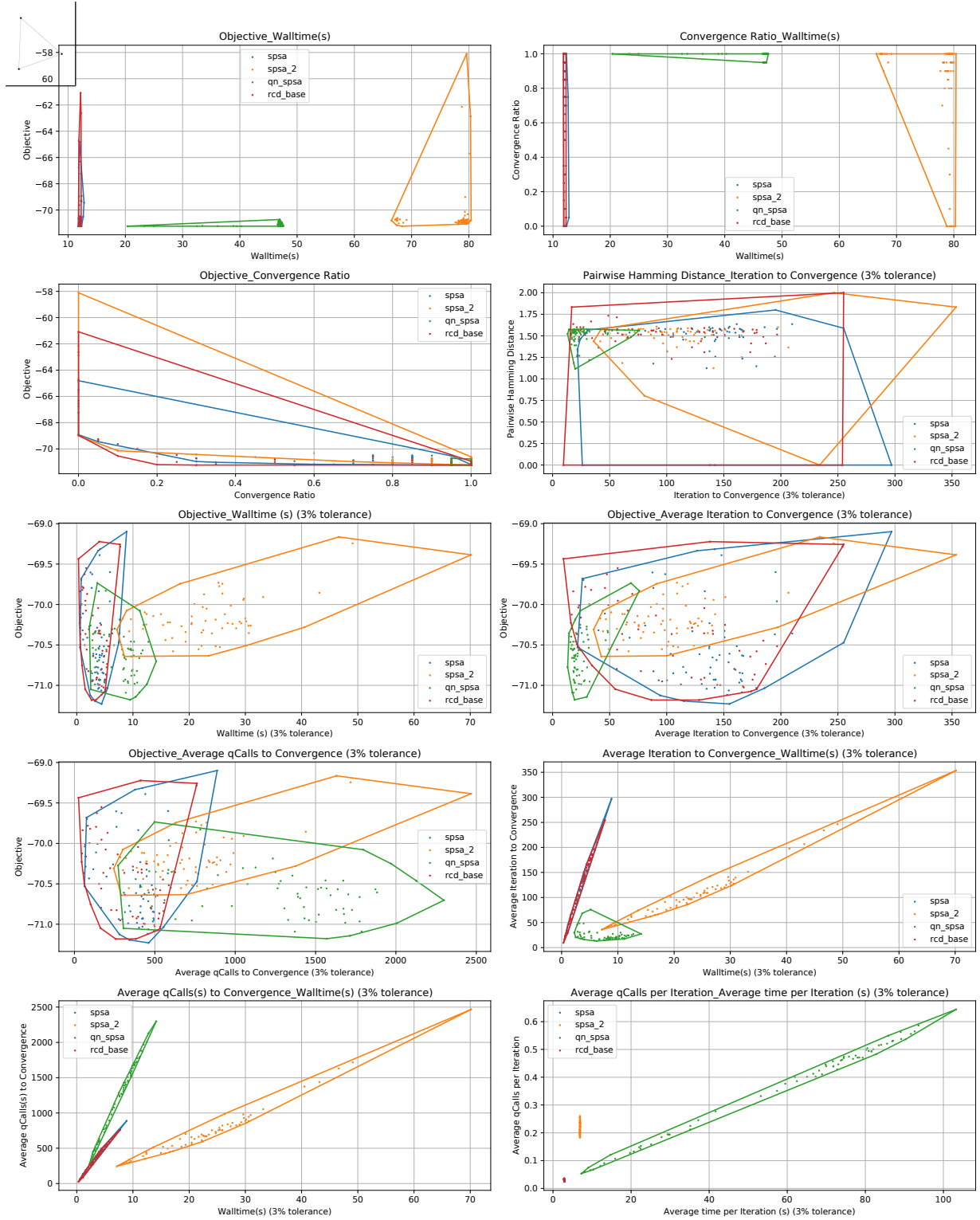


Figure 32: 3 nodes problems, 400 iterations max, stochastic methods on shot-noise, 70 Bayesian sweeps

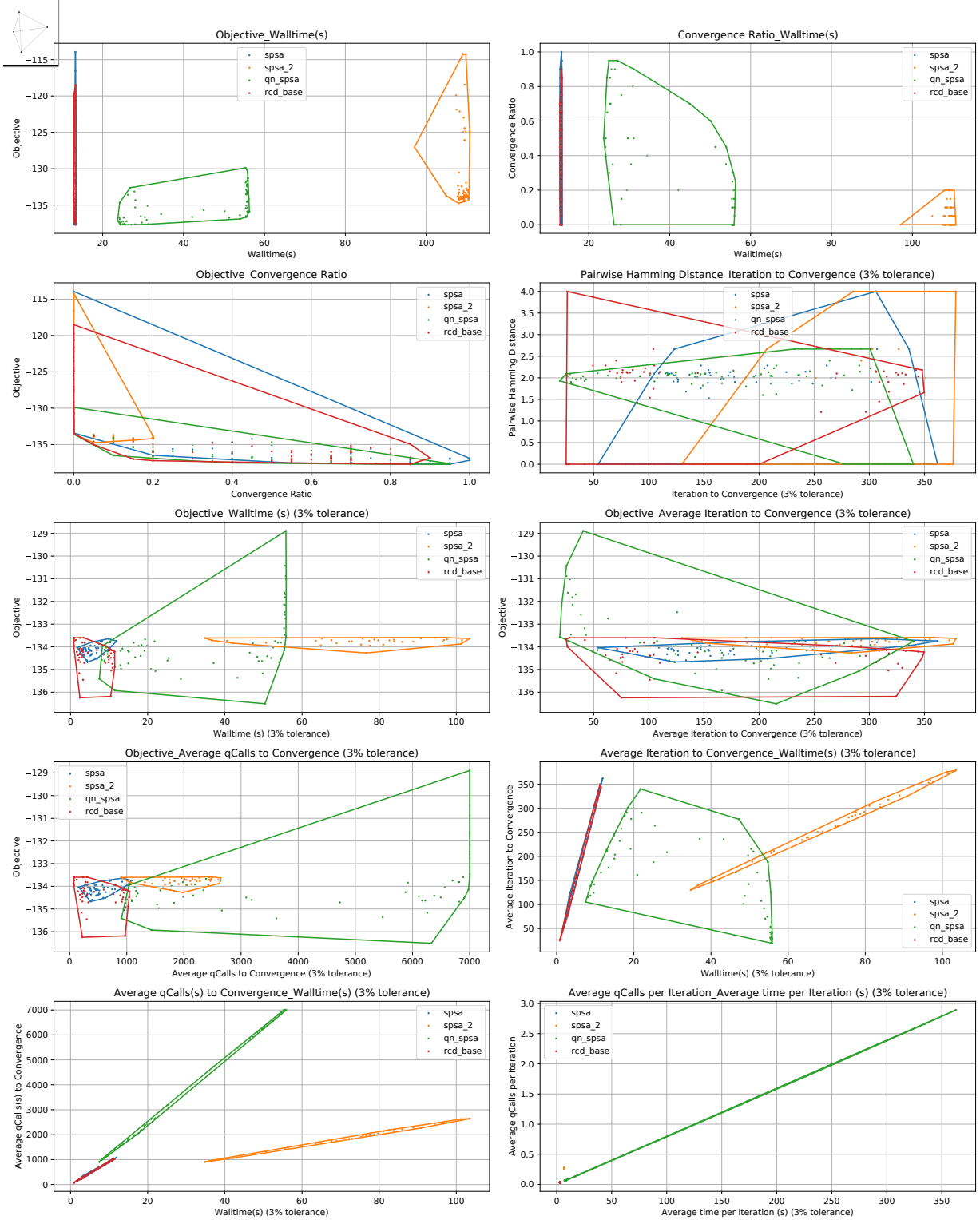


Figure 33: 4 nodes problems, 70 iterations, second order methods noiseless, 70 Bayesian sweeps



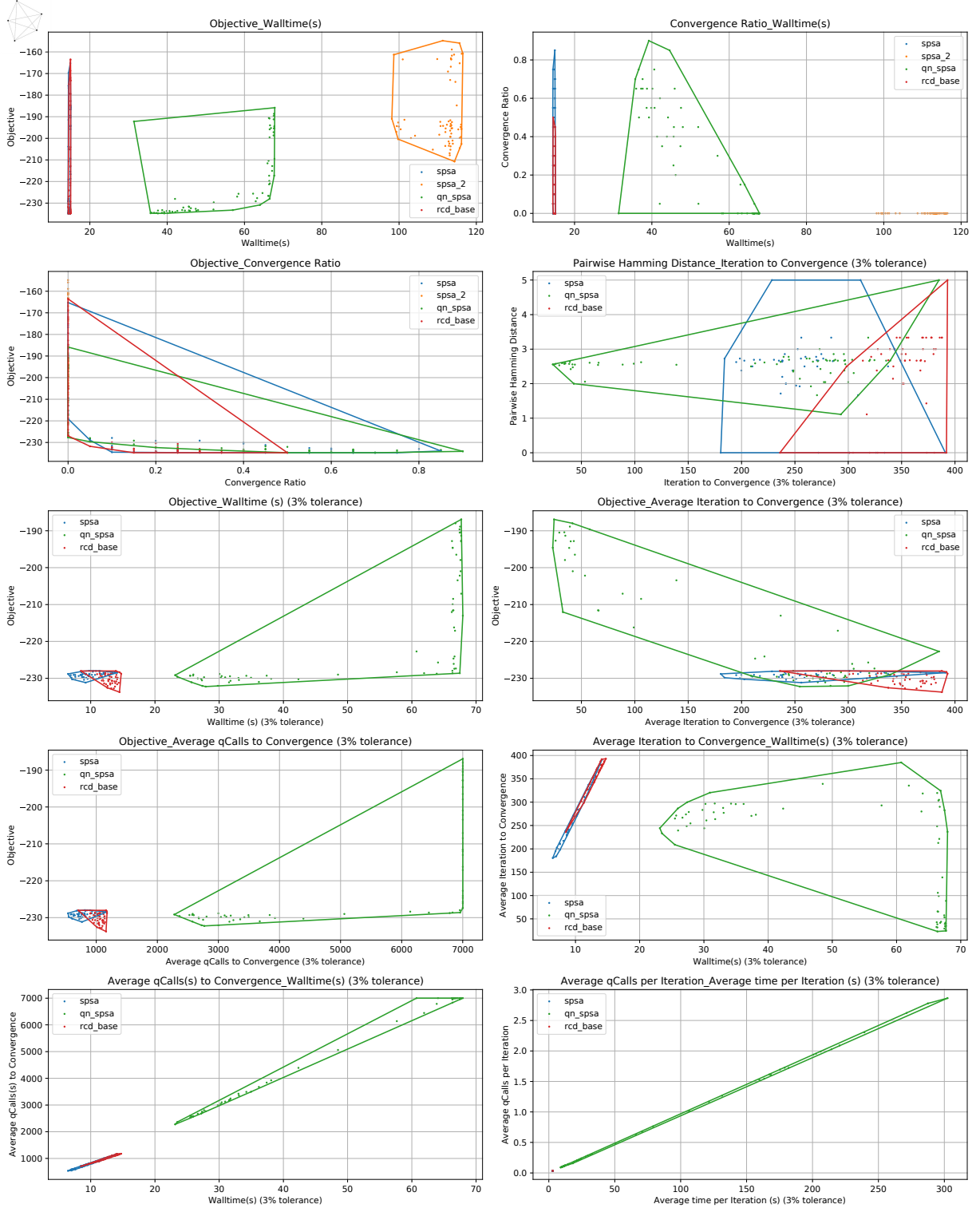


Figure 34: 5 nodes problems, 70 iterations, second order methods noiseless, 70 Bayesian sweeps

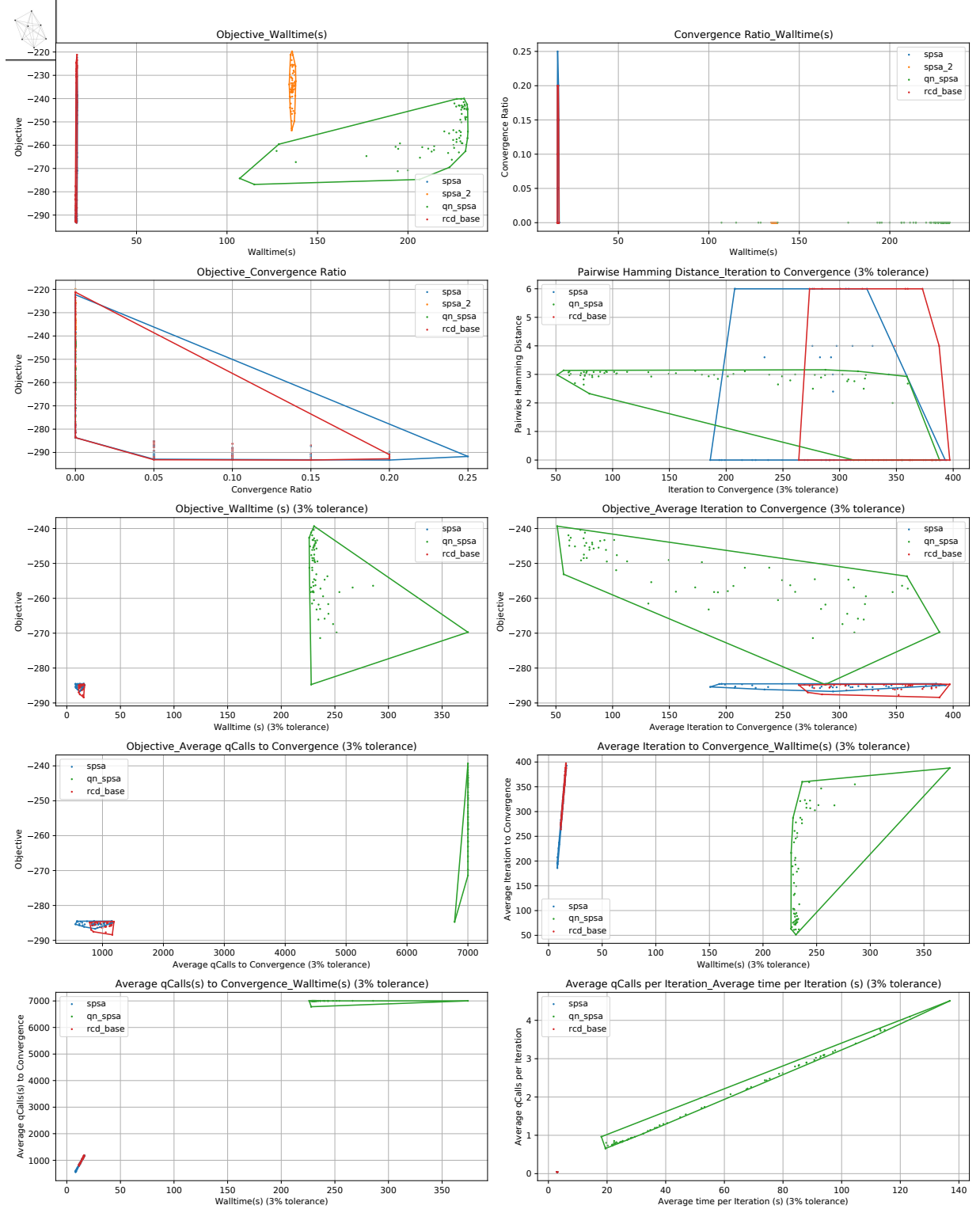


Figure 35: 6 nodes problems, 70 iterations, second order methods noiseless, 70 Bayesian sweeps

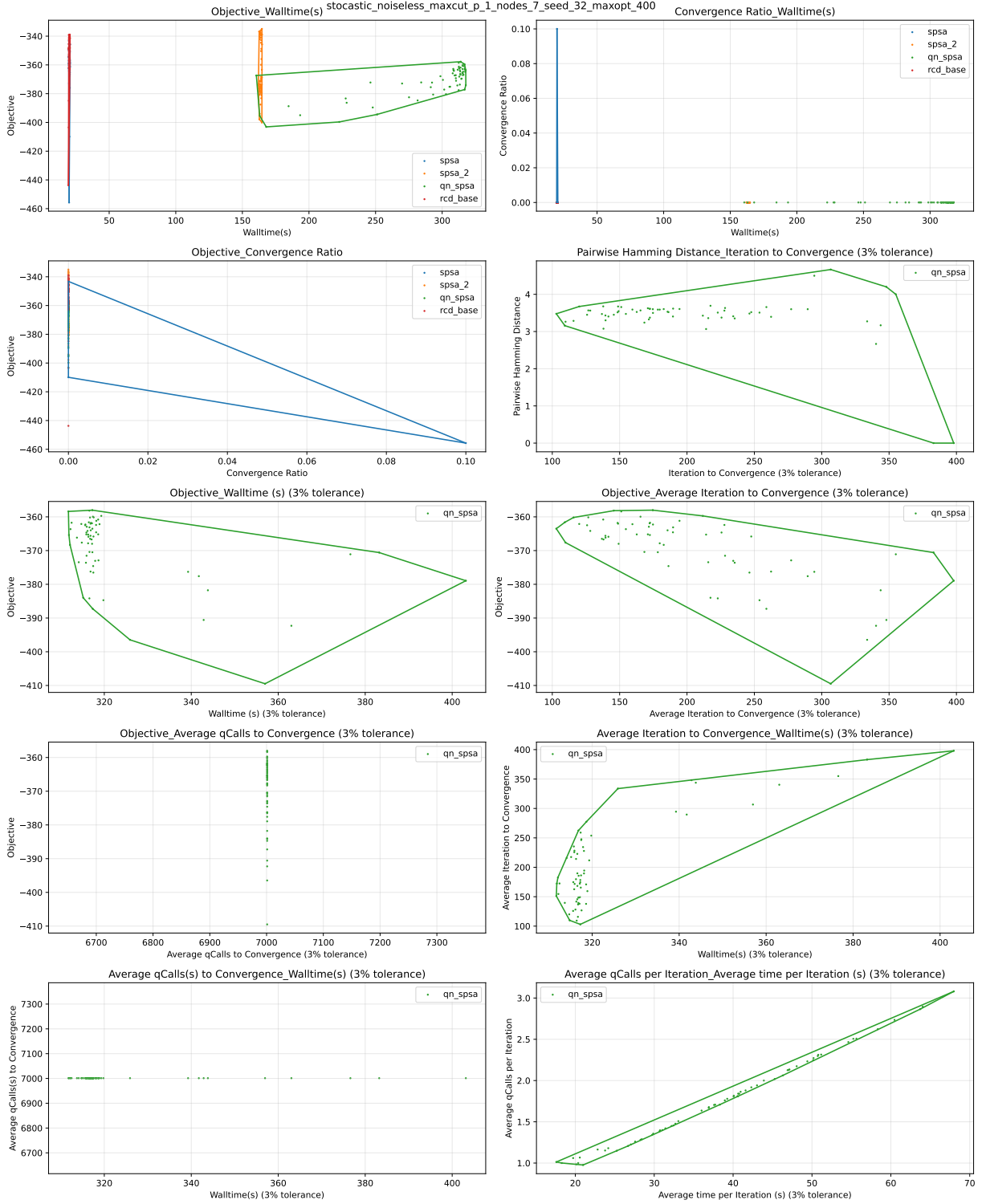


Figure 36: 7 nodes problems, 70 iterations, second order methods noiseless, 70 Bayesian sweeps